TGAL-85-5

FINITE DIFFERENCE CRATERING SUPPORT

Analysis of Regional Data from Cratering and Non-Cratering Nuclear Explosions

I.N. Gupta, K.L. McLaughlin, and R.A. Wagner
Teledyne Geotech Alexandria Laboratories
314 Montgomery Street
Alexandria, Virginia 22314-1581

FEBRUARY 1988

FINAL TECHNICAL REPORT
ARPA ORDER NO.: 5143
PROJECT TITLE: Cratering Explosion Yield Determination
CONTRACT: MDA903-84-C-0289

Approved for Public Release; Distribution Unlimited.

Prepared for:
DEFENSE ADVANCED RESEARCH PROJECTS AGENCY
1400 Wilson Boulevard
Arlington, VA 22209

Monitored by:
DEPARTMENT OF THE ARMY
Defense Supply Service
Room 1D 245, The Pentagon
Washington, D. C. 20310

The views and conclusions contained in this report are those of the authors and should not be interpreted as representing the official policies, either expressed or implied, of the Defense Advanced Research Projects Agency or the U.S. Government.

UNCLASSIFIED
SECURITY CLASSIFICATION OF THIS PAGE

REPORT DOCUMENTATION PAGE

Form Approved
OMB No. 0704-0188
Exp. Date: Jun 30, 1986

1a. REPORT SECURITY CLASSIFICATION UNCLASSIFIED	1b. RESTRICTIVE MARKINGS
2a. SECURITY CLASSIFICATION AUTHORITY	3. DISTRIBUTION / AVAILABILITY OF REPORT Approved for Public Release; Distribution Unlimited.
2b. DECLASSIFICATION / DOWNGRADING SCHEDULE	
4. PERFORMING ORGANIZATION REPORT NUMBER(S) TGAL-85-5	5. MONITORING ORGANIZATION REPORT NUMBER(S)
6a. NAME OF PERFORMING ORGANIZATION Teledyne Geotech Alexandria Laboratories 6b. OFFICE SYMBOL (If applicable)	7a. NAME OF MONITORING ORGANIZATION Defense Supply Service - Washington
6c. ADDRESS (City, State, and ZIP Code) 314 Montgomery Street Alexandria, Virginia	7b. ADDRESS (City, State, and ZIP Code) Room 1D245, The Pentagon Washington, D.C. 20310
8a. NAME OF FUNDING / SPONSORING ORGANIZATION DARPA 8b. OFFICE SYMBOL (If applicable) GSD	9. PROCUREMENT INSTRUMENT IDENTIFICATION NUMBER MDA903-84-C-0289
8c. ADDRESS (City, State, and ZIP Code) 1400 Wilson Boulevard Arlington, VA 22209	10. SOURCE OF FUNDING NUMBERS PROGRAM ELEMENT NO. / PROJECT NO. / TASK NO. / WORK UNIT ACCESSION NO.
11. TITLE (Include Security Classification) Finite Difference Cratering Support	
12. PERSONAL AUTHOR(S) I.N. Gupta, K.L. McLaughlin, R.A. Wagner	
13a. TYPE OF REPORT Final 13b. TIME COVERED FROM Jun 84 TO Jun 85	14. DATE OF REPORT (Year, Month, Day) February 1988 15. PAGE COUNT 53
16. SUPPLEMENTARY NOTATION	

17. COSATI CODES		
FIELD	GROUP	SUB-GROUP
08	11	
17	10	

18. SUBJECT TERMS (Continue on reverse if necessary and identify by block number)
regional phases, cratering explosions, underground nuclear explosions, Pn, Pg, and Lg.

19. ABSTRACT (Continue on reverse if necessary and identify by block number)

A comparison of regional phases generated by contained and cratering nuclear explosions is made by examining the amplitudes of various phases and by spectral analyses. Using Ringdal's maximum likelihood method, in which one can also make use of clipped readings as well as noise measurements, amplitudes of the regional phases Pn, Pg, Lg (corrected for spatial attenuation) and the ratio Pmax/Pa (where Pmax is the largest amplitude in the first 5 sec of Pn and where Pa refers to the "a" phase) were plotted against the known yields of explosions. No systematic distinction could be observed, at regional distances, between cratering and non-cratering explosions at NTS; the excitation of various regional phases appears to depend more on conditions at or near the source than on whether the shot produced a crater or not. We also examined the spectra of Pn on KN-UT records of several Pahute Mesa explosions covering a wide range of scaled depths. The observed modulation of Pn spectra agreed with that expected due to cancellation by pP in only a few instances. A comparison of the Pn spectra of closely spaced explosions suggested that the pP arrivals are probably severely

20. DISTRIBUTION / AVAILABILITY OF ABSTRACT ☒ UNCLASSIFIED/UNLIMITED ☐ SAME AS RPT. ☐ DTIC USERS	21. ABSTRACT SECURITY CLASSIFICATION UNCLASSIFIED
22a. NAME OF RESPONSIBLE INDIVIDUAL Dr. Robert Blandford	22b. TELEPHONE (Include Area Code) 202-694-3145 22c. OFFICE SYMBOL GSD

DD FORM 1473, 84 MAR 83 APR edition may be used until exhausted
All other editions are obsolete

SECURITY CLASSIFICATION OF THIS PAGE
UNCLASSIFIED

Nevada Test Site

cont.

19. (continued)

distorted by the effects of inelastic processes in the source region of large explosions and scattering due to large lateral variations. These two effects may, in most cases, be strong enough not only to obliterate any definite evidence of the classical pP arrival but also mask any differences between cratering and contained explosions recorded at regional distances.

ANALYSIS OF REGIONAL DATA FROM CRATERING AND NON-CRATERING NUCLEAR EXPLOSIONS

SUMMARY

A comparison of regional phases generated by contained and cratering nuclear explosions is made by examining the amplitudes of various phases and by spectral analyses. Using Ringdal's maximum likelihood method, in which one can also make use of clipped readings as well as noise measurements, amplitudes of the regional phases Pn, Pg, Lg (corrected for spatial attenuation) and the ratio Pmax/Pa (where Pmax is the largest amplitude in the first 5 sec of Pn, and where Pa refers to the "a" phase), were plotted against the known yields of explosions. No systematic distinction could be observed, at regional distances, between cratering and non-cratering explosions at NTS; the excitation of various regional phases appears to depend more on conditions at or near the source than on whether the shot produced a crater or not. We also examined the spectra of Pn on KN-UT records of several Pahute Mesa explosions covering a wide range of scaled depths. The observed modulation of Pn spectra agreed with that expected due to cancellation by pP in only a few instances. A comparison of the Pn spectra of closely spaced explosions suggested that the pP arrivals are probably severely distorted by the effects of inelastic processes in the source region of large explosions and by scattering due to large lateral variations. These two effects may, in most cases, be strong enough not only to obliterate any definite evidence of the classical pP arrival but also to mask any differences between cratering and contained explosions recorded at regional distances.

(THIS PAGE INTENTIONALLY LEFT BLANK)

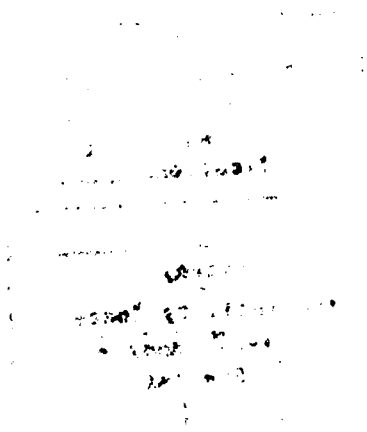

TABLE OF CONTENTS

LIST OF FIGURES

NOTE: Figures 1, 2, and 3 contain data points based on classified yield values and are therefore not included here. These three figures can be seen in Appendix A, TGAL-85-5.

(THIS PAGE INTENTIONALLY LEFT BLANK)

INTRODUCTION

In this study, a comparison of the regional phases generated by contained and cratering nuclear explosions was carried out. The regional phases studied were Pn, Pg, and Lg as well as Pa and Pmax, where Pa refers to the "a" phase and where Pmax is the largest amplitude in the first 5 sec of Pn. Short-period records of explosions at both Yucca Flats and Pahute Mesa regions of the Nevada Test Site were examined at several stations within an epicentral distance of about 20 deg. Most of the analyses was carried out on time-domain measurements. Spectral data from a limited number of explosions were studied in order to understand the generation of regional phases by cratering and non-cratering explosions. The spectra and spectral ratios of Pn were examined since it is especially important to know what possible role pP arrivals play in the make-up of Pn.

TIME-DOMAIN ANALYSES OF REGIONAL PHASES

We analyzed data on regional phases Pn, Pg, and Lg from 4 cratering and 8 nearby contained explosions at NTS. Table 1 lists these 12 explosions along with pertinent information such as the shot medium, shot depth, and depth of water table. Five of these explosions are from the Yucca Flats region of the NTS, including the cratering explosion Sedan. The remaining 7 shots are from Pahute Mesa and include 3 cratering explosions : Palanquin, Cabriolet, and Schooner.

TABLE 1

NTS CRATERING AND CONTAINED EXPLOSIONS USED IN REGIONAL STUDY

No.	Name	Date	Shot Medium (m)	Shot Depth (m)	Depth of Water Table	Location
1	Sedan*	06 July 62	alluvium	194	576	YF
2	Mississippi	05 Oct 62	tuff	494	561	YF
3	Fore	16 Jan 64	tuff	491	556	YF
4	Dub	30 Jun 64	alluvium	259	568	YF
5	Par	09 Oct 64	alluvium	406	594	YF
6	Palanquin*	14 Apr 65	rhyolite	86	488	PM
7	Duryea	14 Apr 66	rhyolite	544	662	PM
8	Cabriolet*	26 Jan 68	rhyolite	52	488	PM
9	Scroll	23 Apr 68	tuff	224	635	PM
10	Chateaugay	28 Jun 68	tuff	617	633	PM
11	Schooner*	08 Dec 68	tuff	111	274	PM
12	Purse	07 May 69	tuff	599	594	PM

*cratering explosion

The regional data examined in this phase of the study came from the Long Range Seismic Measurements (LRSM) stations located within an epicentral distance Δ of about 20°. The largest amplitudes of Pn, Pg, and Lg were read on the vertical component short-period records, and the corresponding ground motion values A, corrected for instrument response, were obtained. These amplitudes were plotted versus yield on a log-log scale for several stations for which a fair amount of data were available. Results for the station KN-UT, shown in Figure 1, are typical of those obtained from other sta-

tions as well. The explosion numbers on plots correspond to those in Table 1. Plots of amplitude versus yield for Pn, Pg, and Lg (Figures 1a, b, and c) have correlation coefficients of 0.79, 0.56, and 0.90, respectively. In other words, Pg has the largest scatter and Lg the least. The strong correlation between Lg amplitudes and the yield of NTS explosions has of course been noted before by several investigators (*e.g.*, Blandford and Klouda, 1980; Nuttli, 1983).

In order to make use of multi-station data that included clipped readings as well as noise measurements, Ringdal's (1976) maximum likelihood estimation method was applied to the regional data. The analysis was limited to observations made within Δ less than 10° because the cratering explosions, with the exception of Sedan, did not produce any observable regional phases at Δ greater than 10°. The Pn, Pg, and Lg amplitudes were corrected for attenuation with distance Δ by using the empirical attenuation rates of $\Delta^{-3.8}$ for Pn (Der *et al.*, 1982) and Δ^{-3} for both Pg and Lg (Blandford *et al.*, 1981; Der *et al.*, 1982). The resulting values of the maximum likelihood magnitudes (arbitrary units) for Pn, Pg, and Lg are given in Table 2 and plotted versus log yield in Figures 2a,b, and c, respectively. The explosion numbers again correspond to those in Table 1. The correlation coefficients for the three plots are 0.81, 0.80, and 0.87, respectively. These figures again indicate better correlation with yield for Lg than for Pn or Pg. Furthermore, there is again no clear distinction between the cratering and contained explosion populations. In fact, the same explosions seem to have abnormally high or low amplitudes on all phases (Pn, Pg, and Lg). Specifically, explosions numbered 6, 7, 8, and 12 have larger than average values for nearly all three phases whereas explosions 1, 4, and 5 have lower than average values. Explosions 6, 7, and 8 were in rhyolite (see Table 1), which is expected to provide better coupling than alluvium or tuff, the shot medium for the other explosions. Note that in Table 1, explosion 12 (Purse) is the only one with shot point below the water table, which can also lead to better coupling or larger amplitudes. Similarly, the explosions 1, 4, and 5 have generally lower than average amplitudes on all three phases, and this could be because these are the only explosions in allu-

vium (above the water table), which is known to provide low coupling. It seems therefore that the amplitudes of regional phases are mainly controlled by the characteristics of the shot medium and not to any significant extent by whether the explosion is cratering or contained. The relatively better correlation between yield and Lg amplitudes (Figure 2c) indicates that Lg is considerably less sensitive to the effects of differences in coupling properties than are the other two phases Pn and Pg (Figures 2a and 2b).

TABLE 2

RINGDAL'S MAXIMUM-LIKELIHOOD ESTIMATES

No.	Name	m_b(Pn)	m_b(Pg)	m_b(Lg)	log(Pmax/Pa)
1	Sedan*	12.01	10.59	10.71	1.15
2	Mississippi	12.56	11.19	11.17	1.31
3	Fore	12.46	11.18	11.21	1.12
4	Dub	11.11	9.97	9.86	0.68
5	Par	11.63	10.46	10.52	0.79
6	Palanquin*	11.61	10.44	10.26	0.78
7	Duryea	12.94	11.52	11.27	1.14
8	Cabriolet*	11.40	10.08	10.02	0.61
9	Scroll	11.38	10.16	9.79	0.89
10	Chateaugay	12.94	11.87	11.26	0.82
11	Schooner*	12.05	10.74	10.85	0.99
12	Purse	13.41	12.13	11.84	1.14

*cratering explosion

All available regional data for epicentral distances less than 10° were also used to measure amplitudes of the Pa and Pmax phases, where Pa refers to the "a" phase and where Pmax is the largest amplitude in the first 5 sec of Pn. The maximum-likelihood method was applied to all available values of log (Pmax/Pa) for each explosion; the resulting values are also given in Table 2. A plot of the resulting maximum-likelihood ratio Pmax/Pa versus explosion yield (on log-log scale) for these explosions is shown in Figure 3. The least squares linear regression relationship (dashed line) has a mean slope of 0.264 and correlation coefficient of only 0.768; the scatter in the data seems too large to indi-

cate a definite linear relationship. Moreover, there appears to be no clear separation between the cratering and non-cratering explosion populations.

DIGITAL DATA AND SPECTRAL ANALYSES

Short-period, three-component digital data from a selected number of explosions, recorded at the LRSM stations KN-UT and MN-NV, were examined in order to understand some of the complexity of regional phases. Both cratering and non-cratering explosions at various depths were studied. The explosions are listed in Table 3, which also includes information on yield and scaled depth (defined as $h/W^{1/3}$, where h is the depth [m] and W is the yield [kt]). The yield values are from Springer and Kinnaman (1971) except for Buteo. The scaled depth is a measure of whether an explosion is over-buried or underburied or "normal" (most U. S. contained explosions have scaled depths of about 150 $m/kt^{1/3}$). Available three-component records of these 7 explosions at KN-UT and MN-NV are shown in Figures 4 and 5, respectively.

TABLE 3

PAHUTE MESA EXPLOSIONS USED IN SPECTRAL ANALYSES

No.	Name	Date	Shot Medium	Shot Depth (m)	Depth of Water Table	Yield (kt)	Scaled Depth#
1	Buteo	12 May 65	tuff	696	660	-	-
2	Rex	24 Feb 66	tuff	671	642	16	266
3	Duryea	14 Apr 66	rhyolite	544	662	65	135
4	Scotch	23 May 67	tuff	977	672	150	184
5	Cabriolet*	26 Jan 68	rhyolite	52	488	2.3	39
6	Schooner*	8 Dec 68	tuff	111	274	35	34
7	Benham	19 Dec 68	tuff	1402	641	1100	136

* cratering explosion

$h/W^{1/3}$ where h is depth [m] and W is yield [kt]

The spectra of Pn at KN-UT, obtained by taking a window of 6.4 sec length and applying a 10% cosine taper, are shown in Figure 6. The spectra of samples of noise, taken immediately preceding the Pn window, are included in each figure. Similar spectra of Pn at MN-NV could not be obtained because of the lack of a sufficiently long time window separating the Pn and Pg arrivals (see Figure 5).

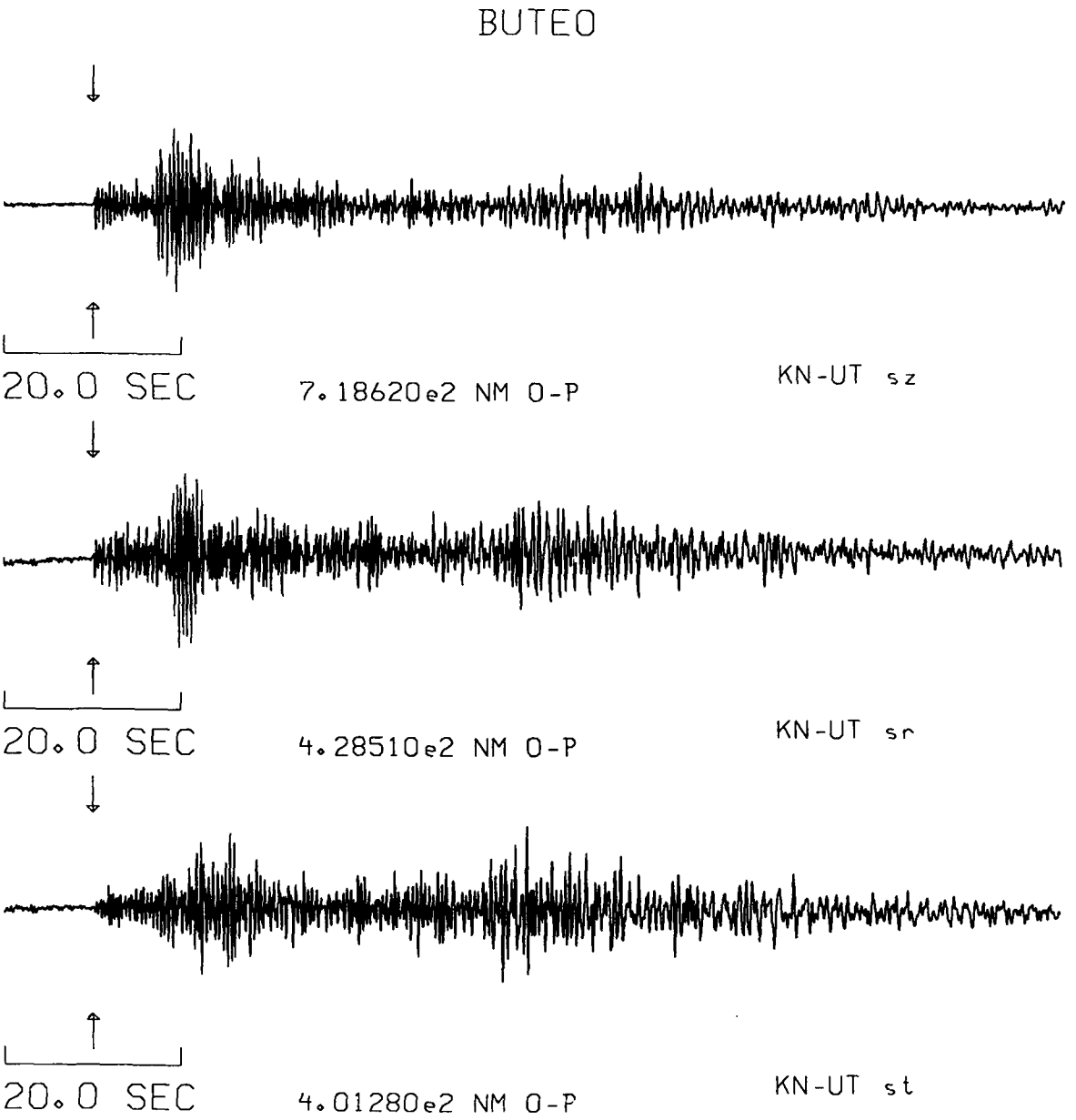

Figure 4. Three-component, short-period records of the seven explosions listed in Table III at the LRSM station KN-UT. The records for each explosion show the vertical (top trace), radial (middle trace), and transverse (bottom trace) motions, respectively. The data are calibrated and the largest zero-to-peak amplitudes are given in nanometers (NM).

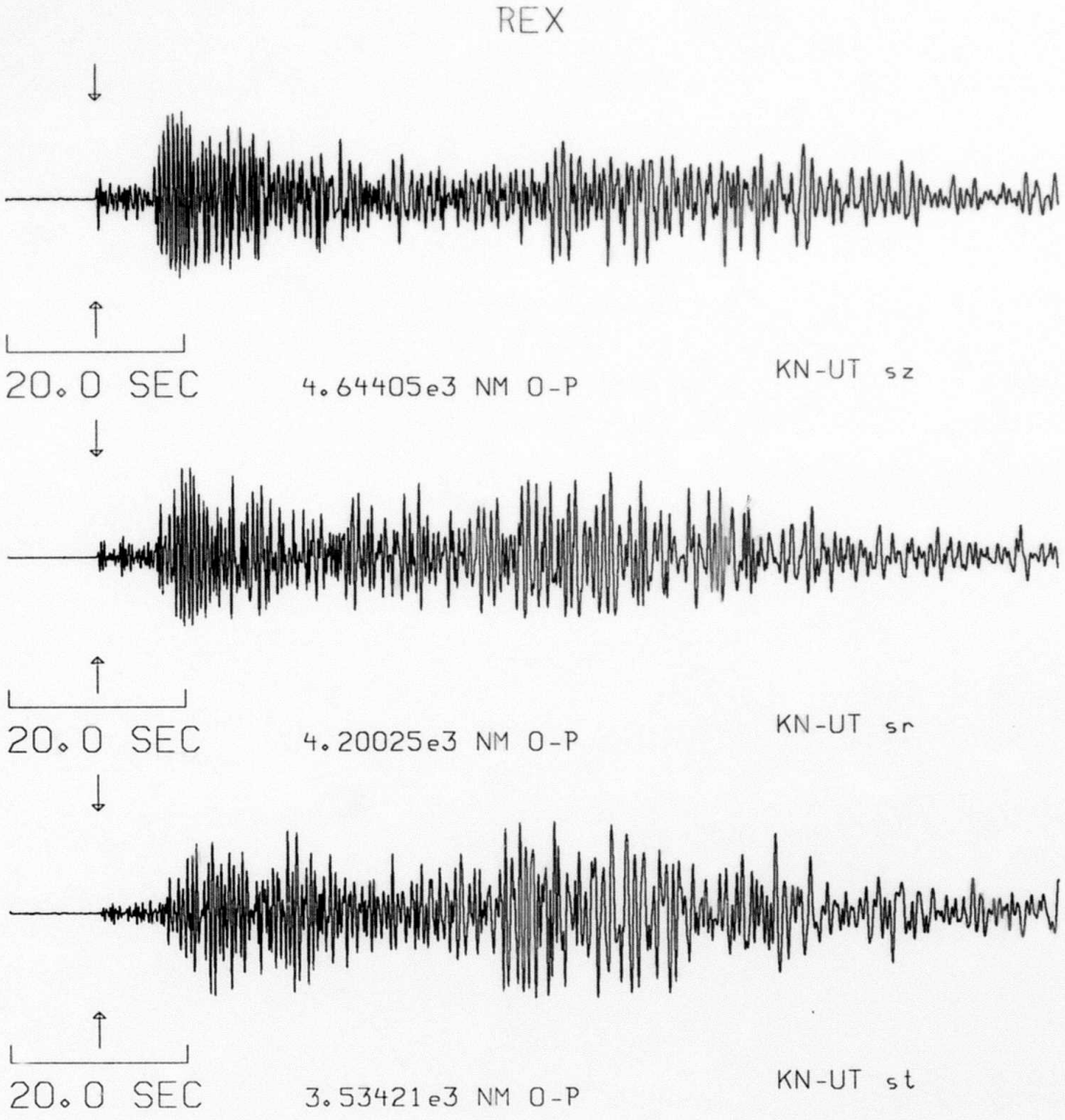

Figure 4. Continued. Three-component, short-period records of the seven explosions listed in Table III at the LRSM station KN-UT. The records for each explosion show the vertical (top trace), radial (middle trace), and transverse (bottom trace) motions, respectively. The data are calibrated and the largest zero-to-peak amplitudes are given in nanometers (NM).

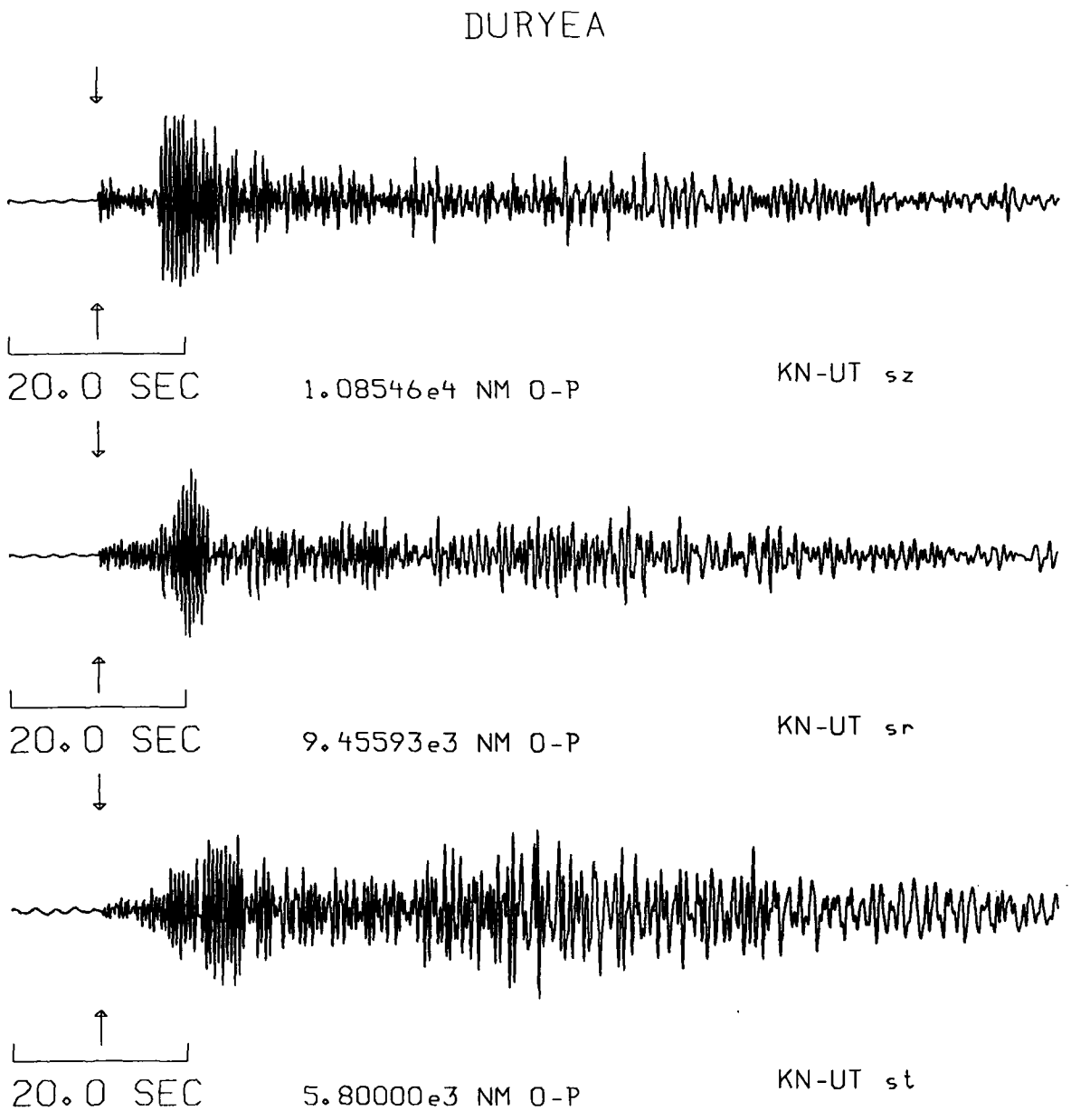

Figure 4. Continued. Three-component, short-period records of the seven explosions listed in Table III at the LRSM station KN-UT. The records for each explosion show the vertical (top trace), radial (middle trace), and transverse (bottom trace) motions, respectively. The data are calibrated and the largest zero-to-peak amplitudes are given in nanometers (NM).

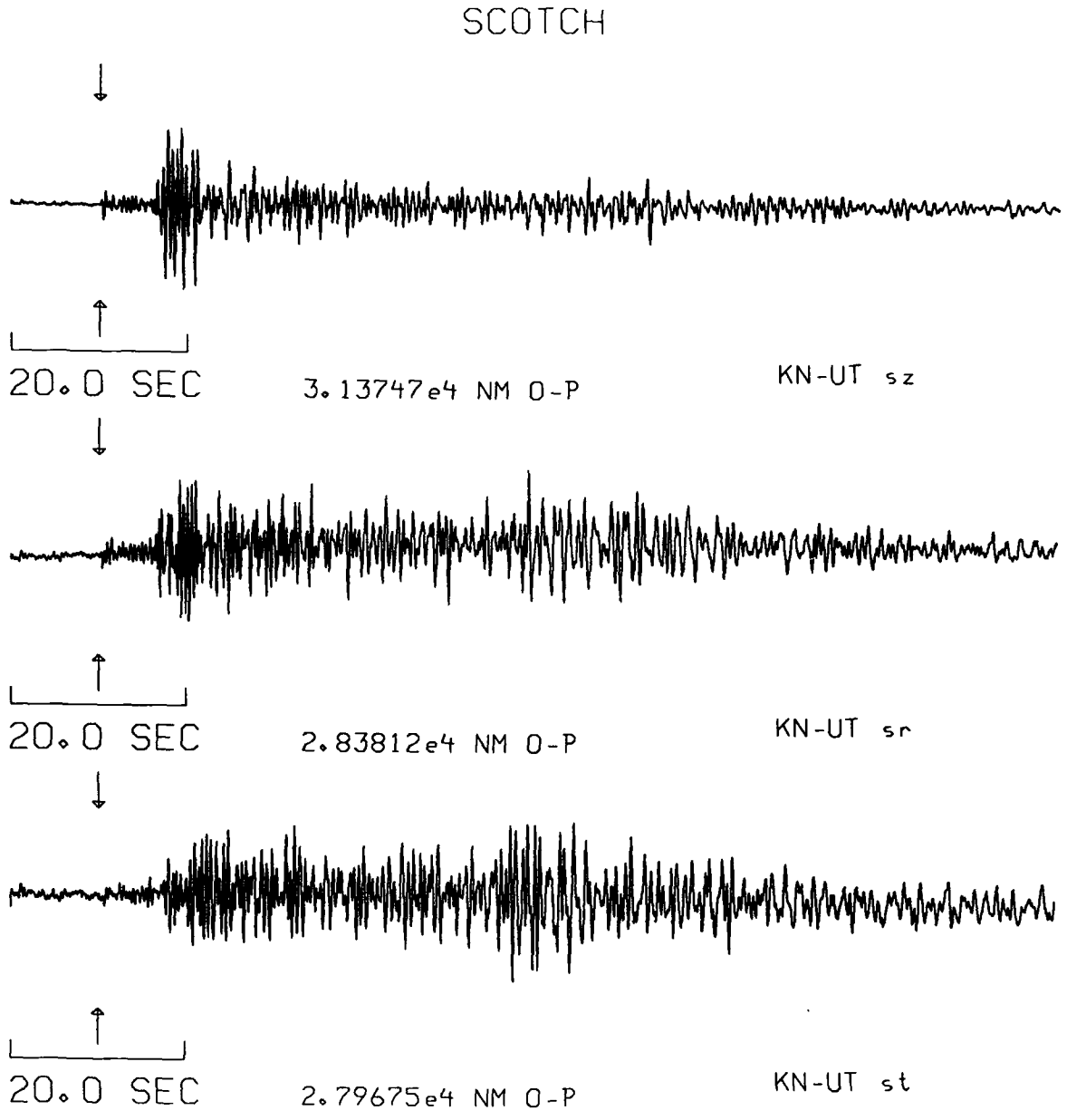

Figure 4. Continued. Three-component, short-period records of the seven explosions listed in Table III at the LRSM station KN-UT. The records for each explosion show the vertical (top trace), radial (middle trace), and transverse (bottom trace) motions, respectively. The data are calibrated and the largest zero-to-peak amplitudes are given in nanometers (NM).

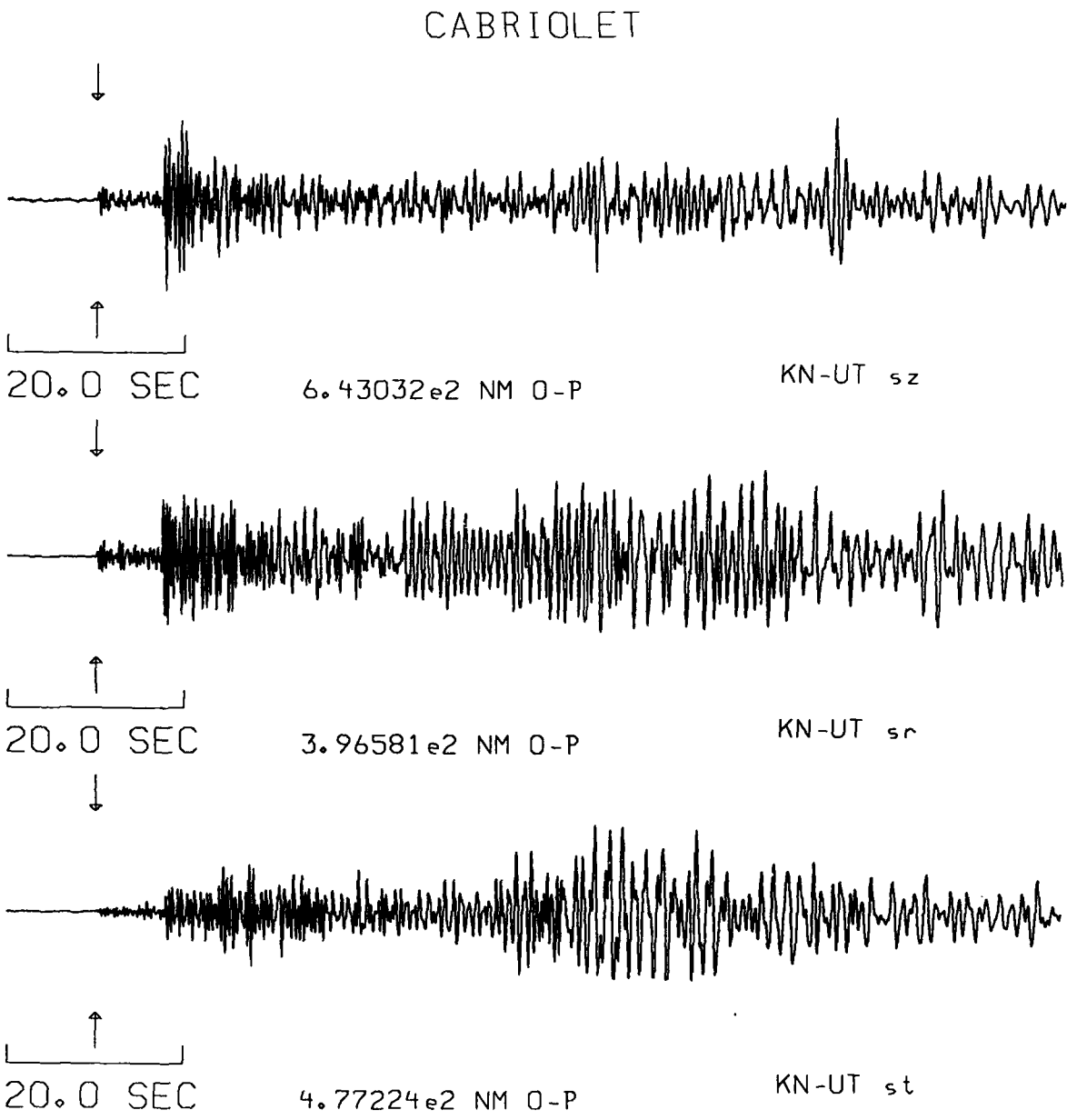

Figure 4. Continued. Three-component, short-period records of the seven explosions listed in Table III at the LRSM station KN-UT. The records for each explosion show the vertical (top trace), radial (middle trace), and transverse (bottom trace) motions, respectively. The data are calibrated and the largest zero-to-peak amplitudes are given in nanometers (NM).

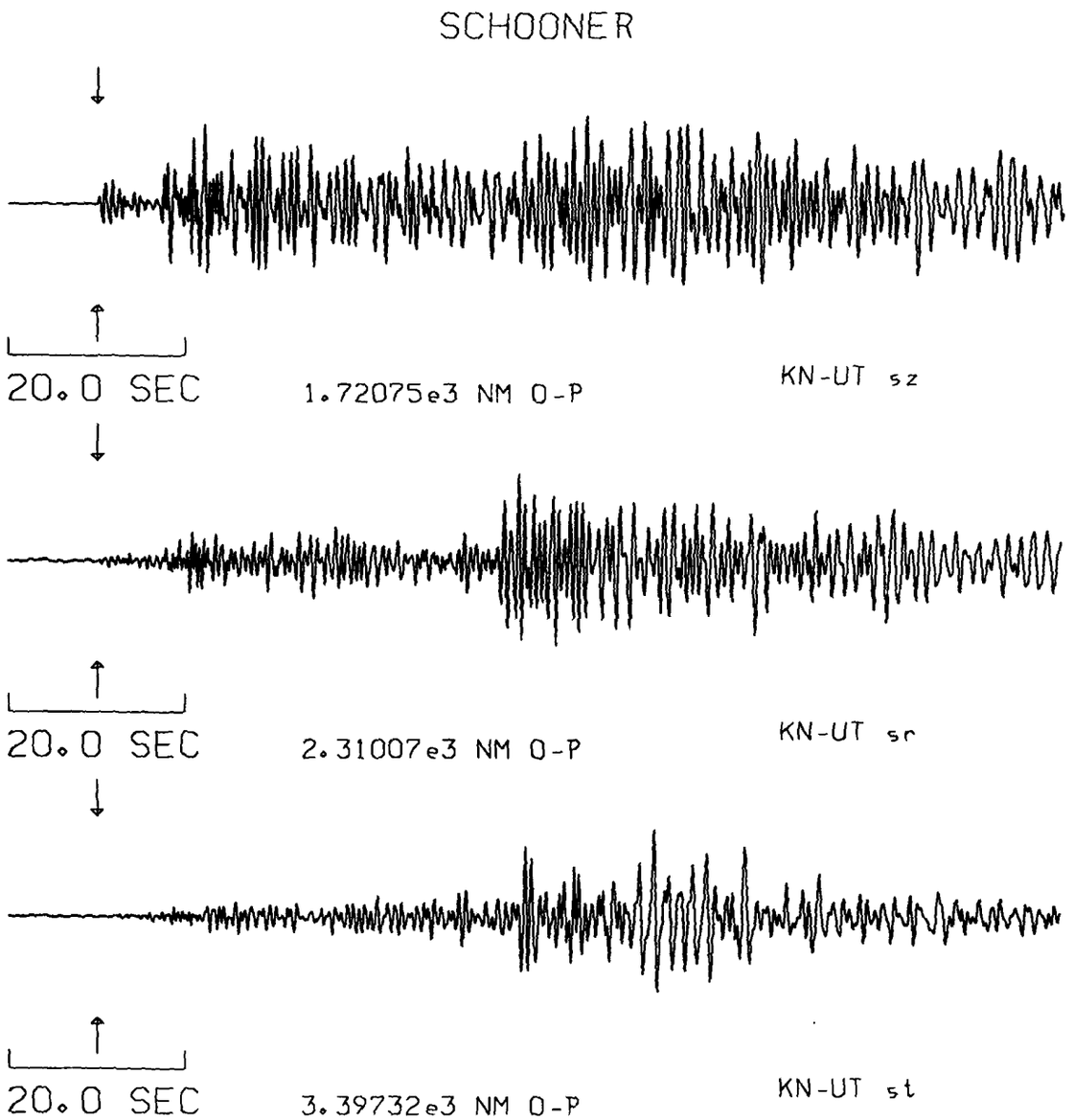

Figure 4. Continued. Three-component, short-period records of the seven explosions listed in Table III at the LRSM station KN-UT. The records for each explosion show the vertical (top trace), radial (middle trace), and transverse (bottom trace) motions, respectively. The data are calibrated and the largest zero-to-peak amplitudes are given in nanometers (NM).

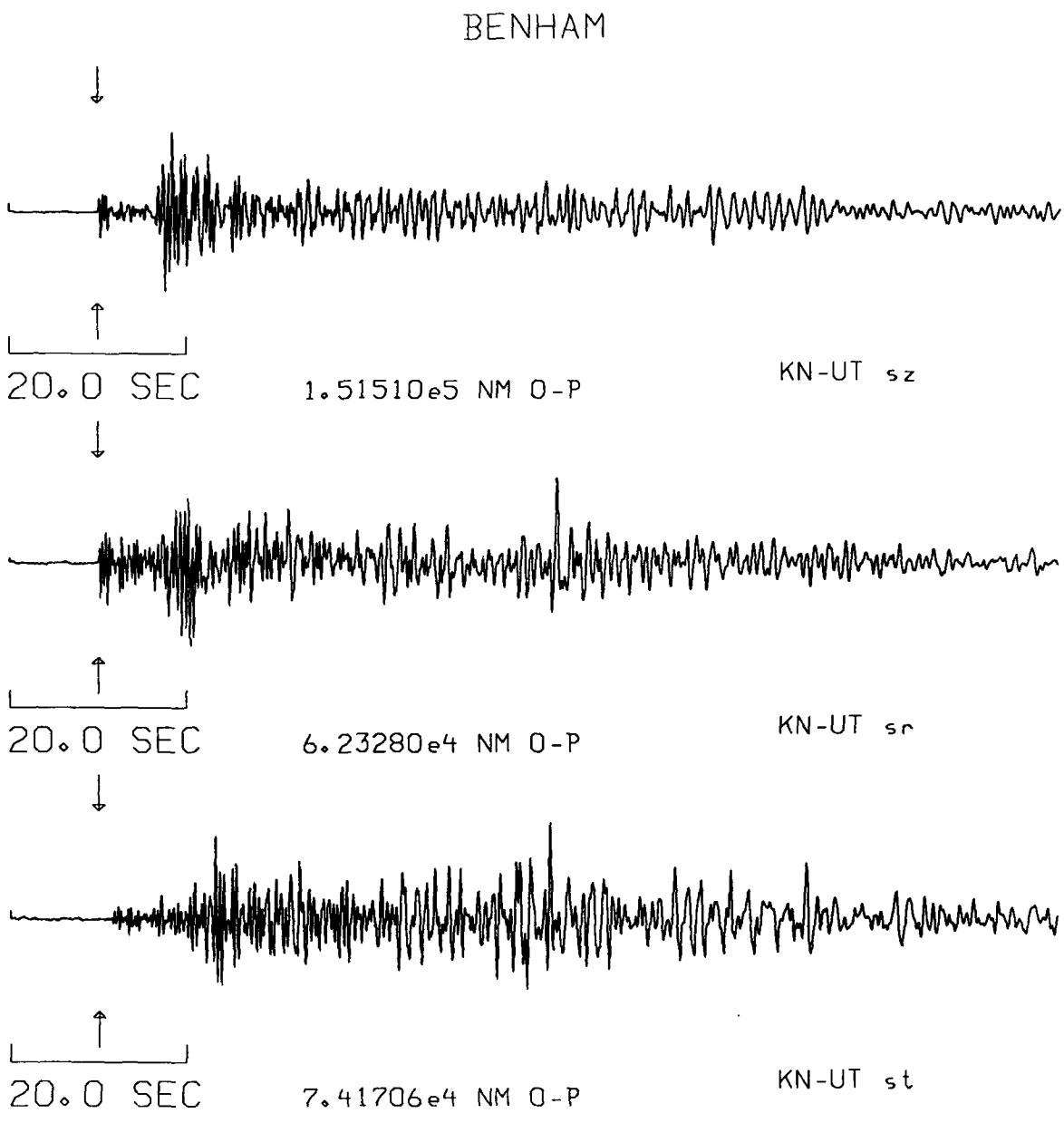

Figure 4. Continued. Three-component, short-period records of the seven explosions listed in Table III at the LRSM station KN-UT. The records for each explosion show the vertical (top trace), radial (middle trace), and transverse (bottom trace) motions, respectively. The data are calibrated and the largest zero-to-peak amplitudes are given in nanometers (NM).

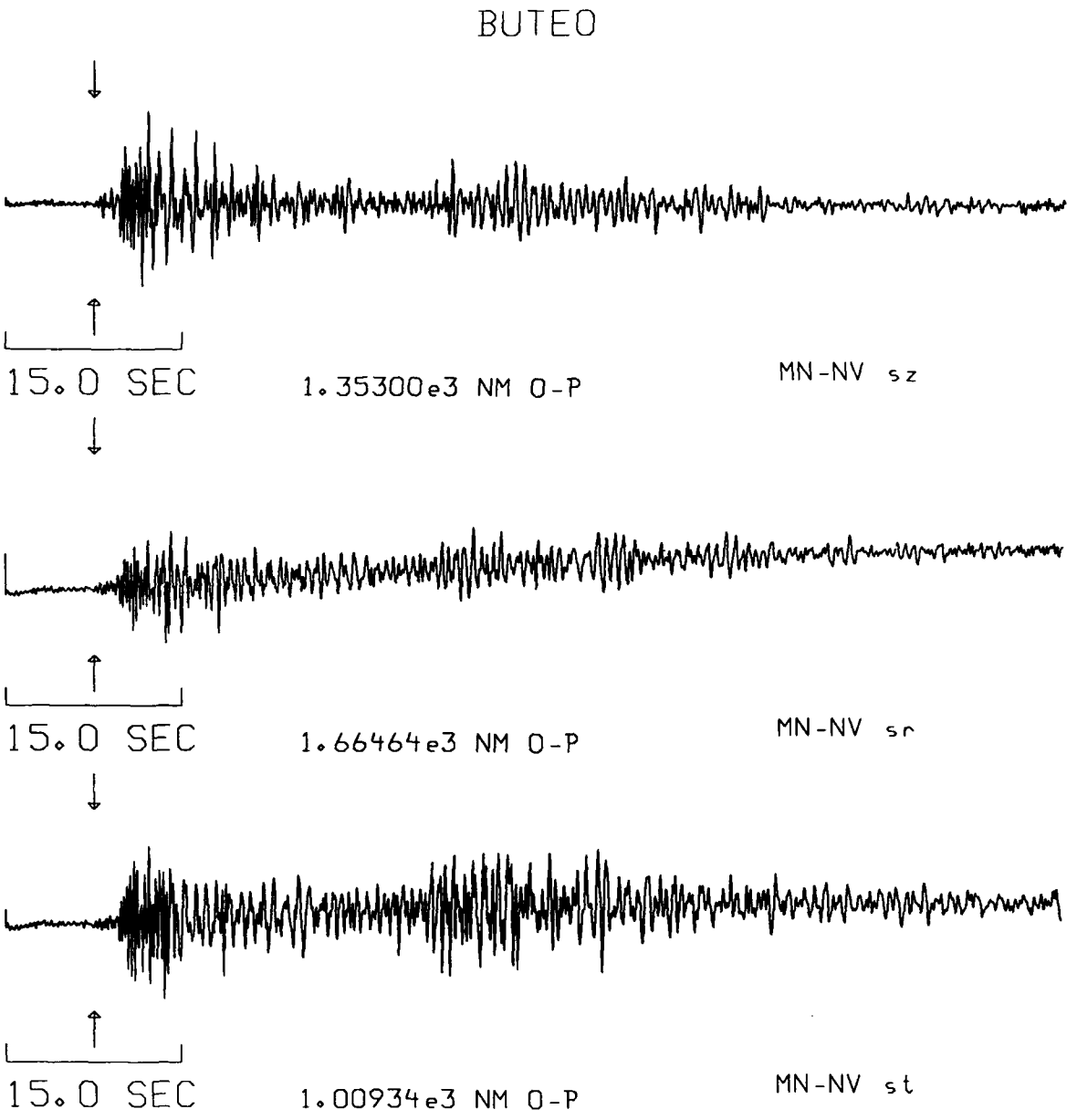

Figure 5. Three-component, short-period records of six out of the seven explosions listed in Table III (i.e. all except Schooner) at the LRSM station MN-NV. The records for each explosion show the vertical (top trace), radial (middle trace), and transverse (bottom trace) motions, respectively. The data are calibrated and the largest zero-to-peak amplitudes are given in nanometers (NM).

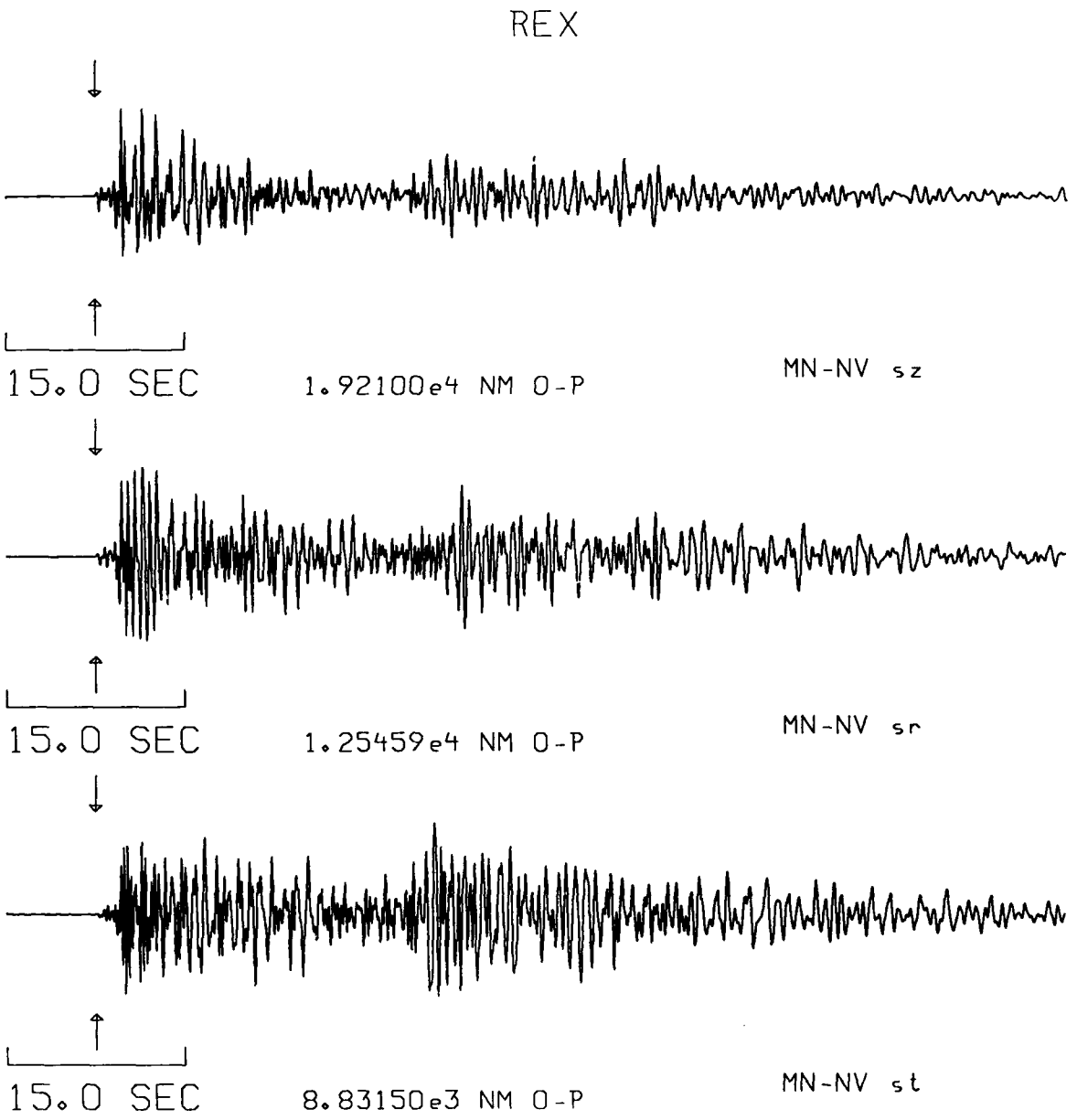

Figure 5. Continued. Three-component, short-period records of six out of the seven explosions listed in Table III (i.e. all except Schooner) at the LRSM station MN-NV. The records for each explosion show the vertical (top trace), radial (middle trace), and transverse (bottom trace) motions, respectively. The data are calibrated and the largest zero-to-peak amplitudes are given in nanometers (NM).

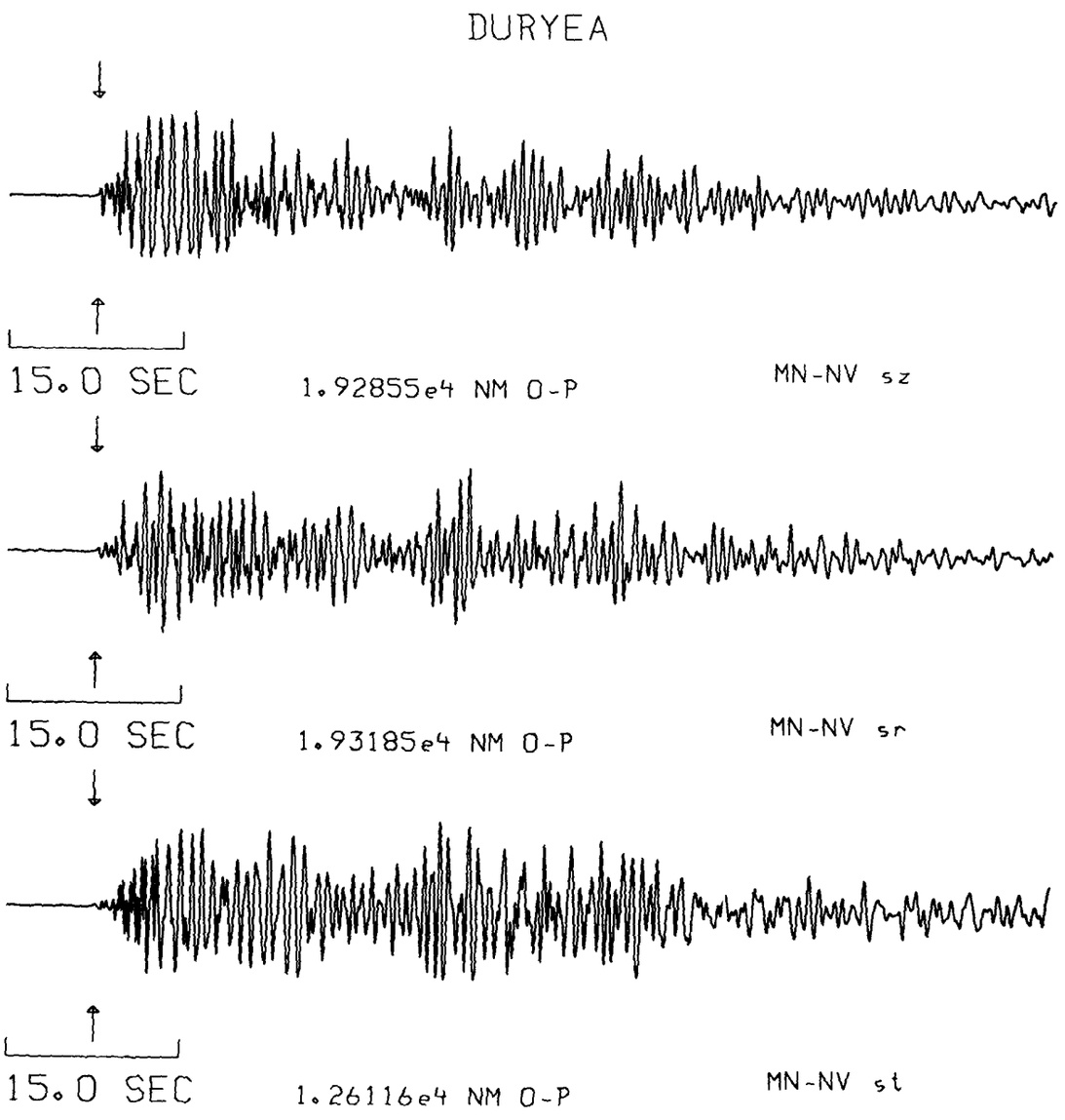

Figure 5. Continued. Three-component, short-period records of six out of the seven explosions listed in Table III (i.e. all except Schooner) at the LRSM station MN-NV. The records for each explosion show the vertical (top trace), radial (middle trace), and transverse (bottom trace) motions, respectively. The data are calibrated and the largest zero-to-peak amplitudes are given in nanometers (NM).

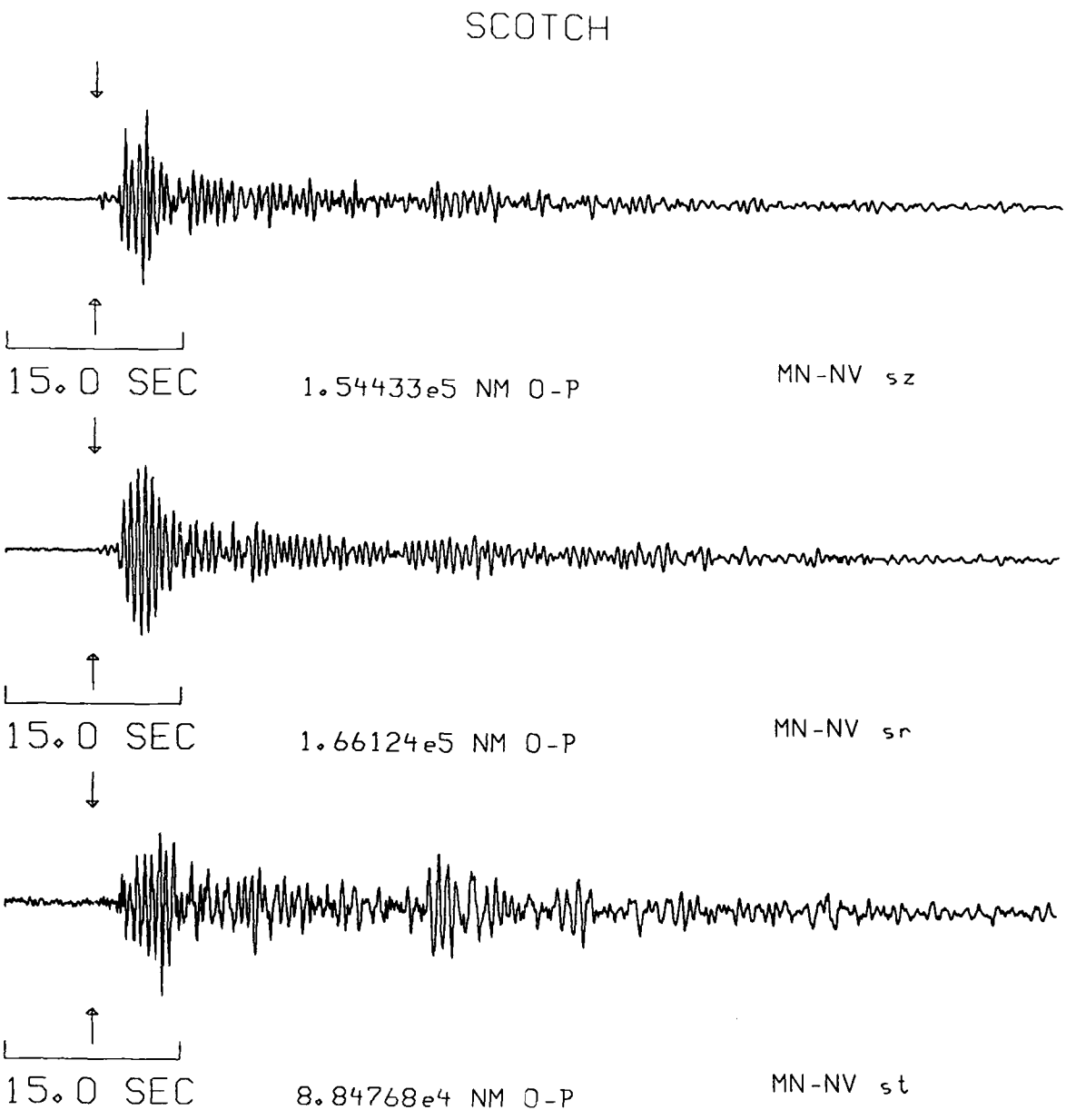

Figure 5. Continued. Three-component, short-period records of six out of the seven explosions listed in Table III (i.e. all except Schooner) at the LRSM station MN-NV. The records for each explosion show the vertical (top trace), radial (middle trace), and transverse (bottom trace) motions, respectively. The data are calibrated and the largest zero-to-peak amplitudes are given in nanometers (NM).

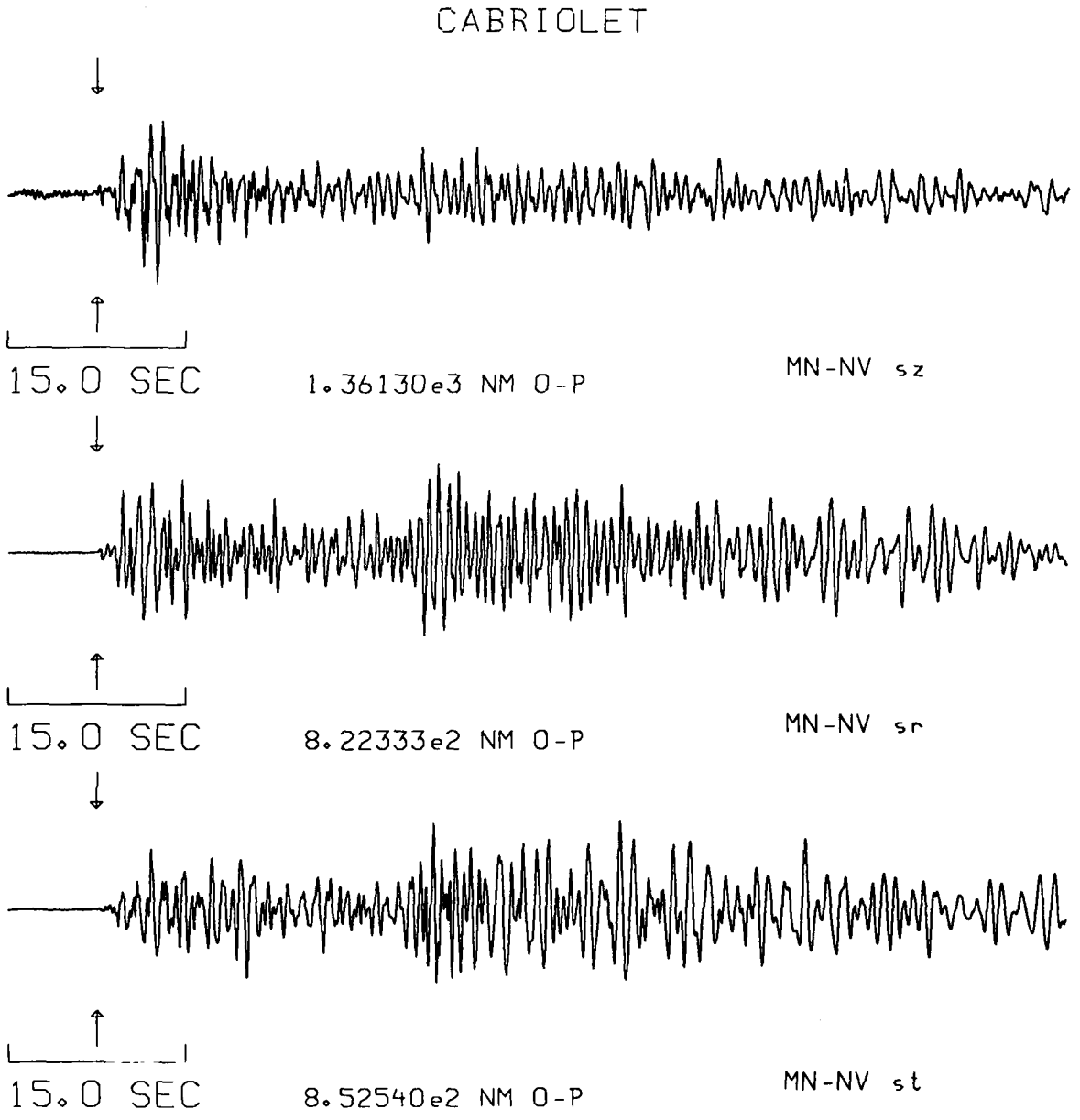

Figure 5. Continued. Three-component, short-period records of six out of the seven explosions listed in Table III (i.e. all except Schooner) at the LRSM station MN-NV. The records for each explosion show the vertical (top trace), radial (middle trace), and transverse (bottom trace) motions, respectively. The data are calibrated and the largest zero-to-peak amplitudes are given in nanometers (NM).

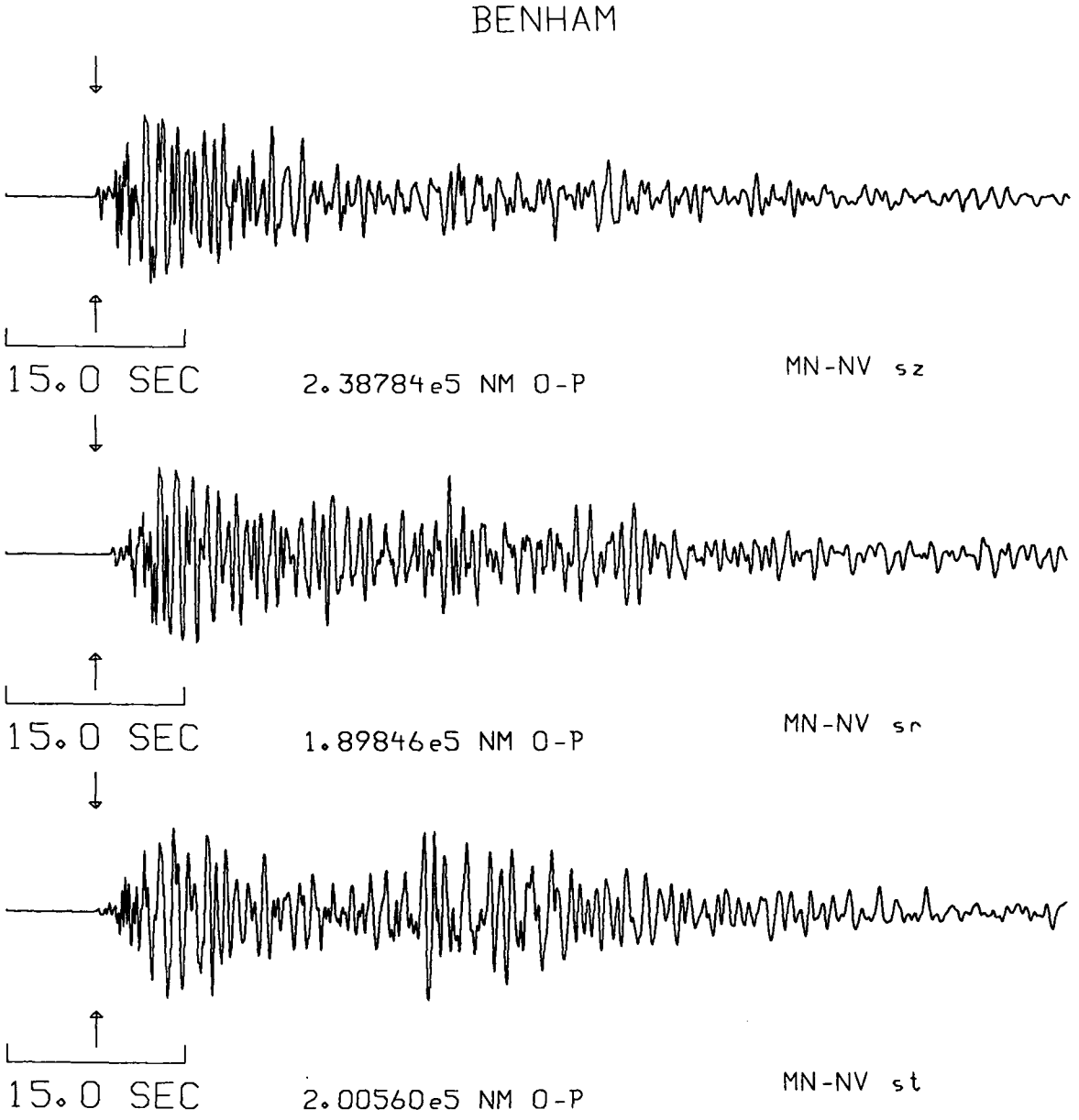

Figure 5. Continued. Three-component, short-period records of six out of the seven explosions listed in Table III (i.e. all except Schooner) at the LRSM station MN-NV. The records for each explosion show the vertical (top trace), radial (middle trace), and transverse (bottom trace) motions, respectively. The data are calibrated and the largest zero-to-peak amplitudes are given in nanometers (NM).

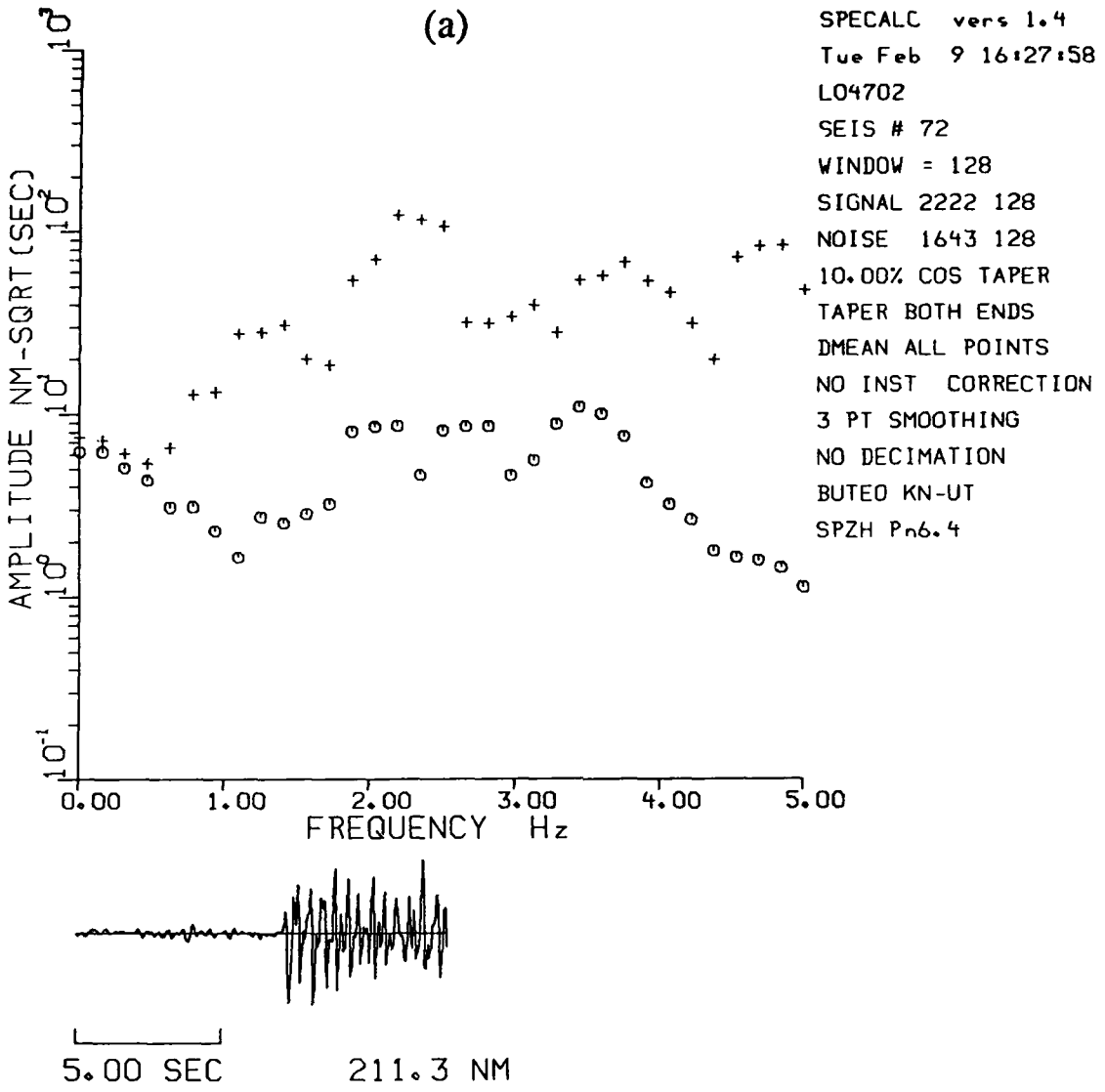

Figure 6. Vertical-component displacement amplitude spectra (symbol +), not corrected for instrument response, of Pn (based on 6.4 sec long window with 10% cosine taper) recorded at KN-UT for the seven explosions listed in Table III. Spectra of an equal window length of noise are also included (symbol ⊙).

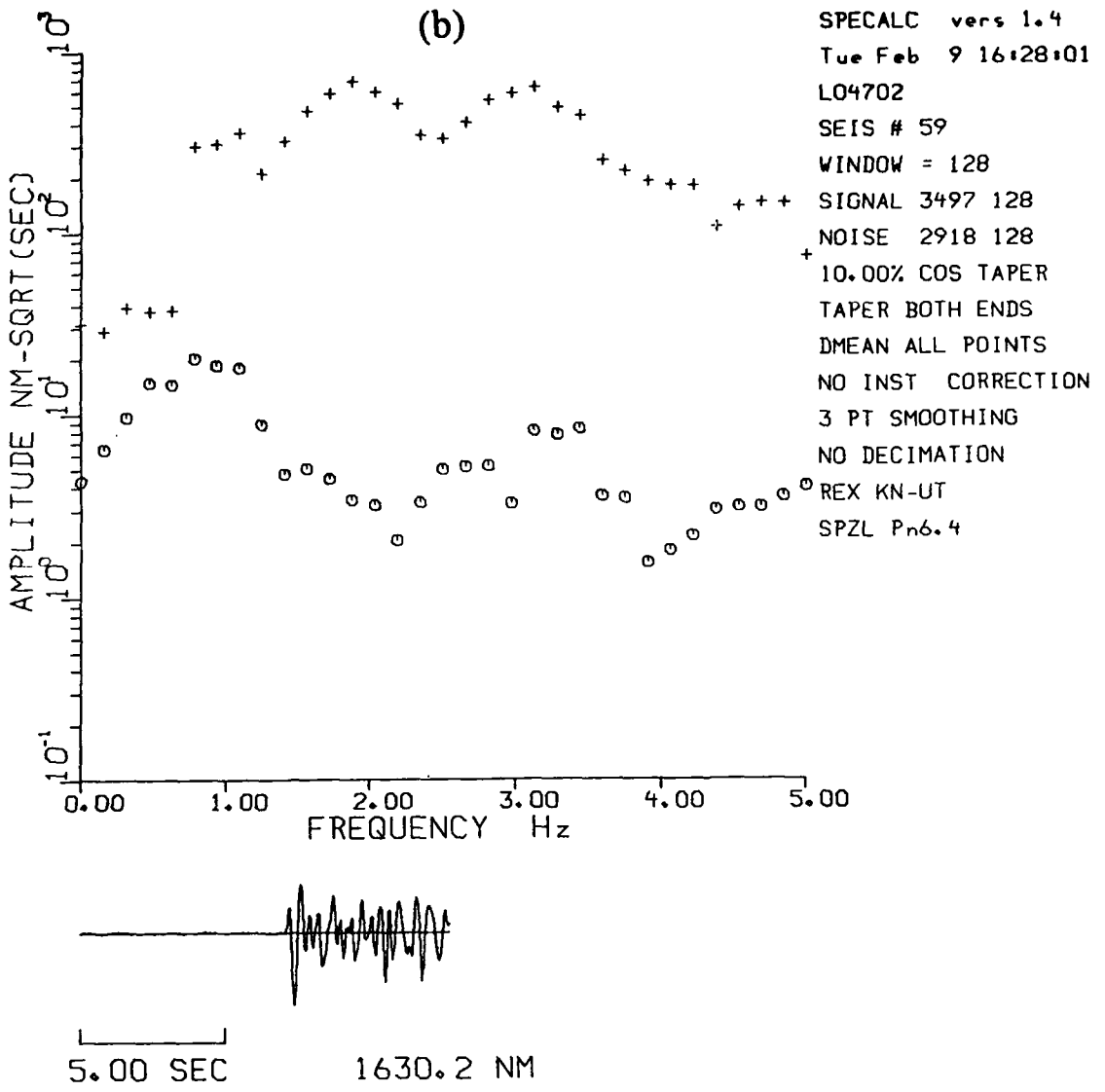

Figure 6. Continued. Vertical-component displacement amplitude spectra (symbol +), not corrected for instrument response, of Pn (based on 6.4 sec long window with 10% cosine taper) recorded at KN-UT for the seven explosions listed in Table III. Spectra of an equal window length of noise are also included (symbol ⊙).

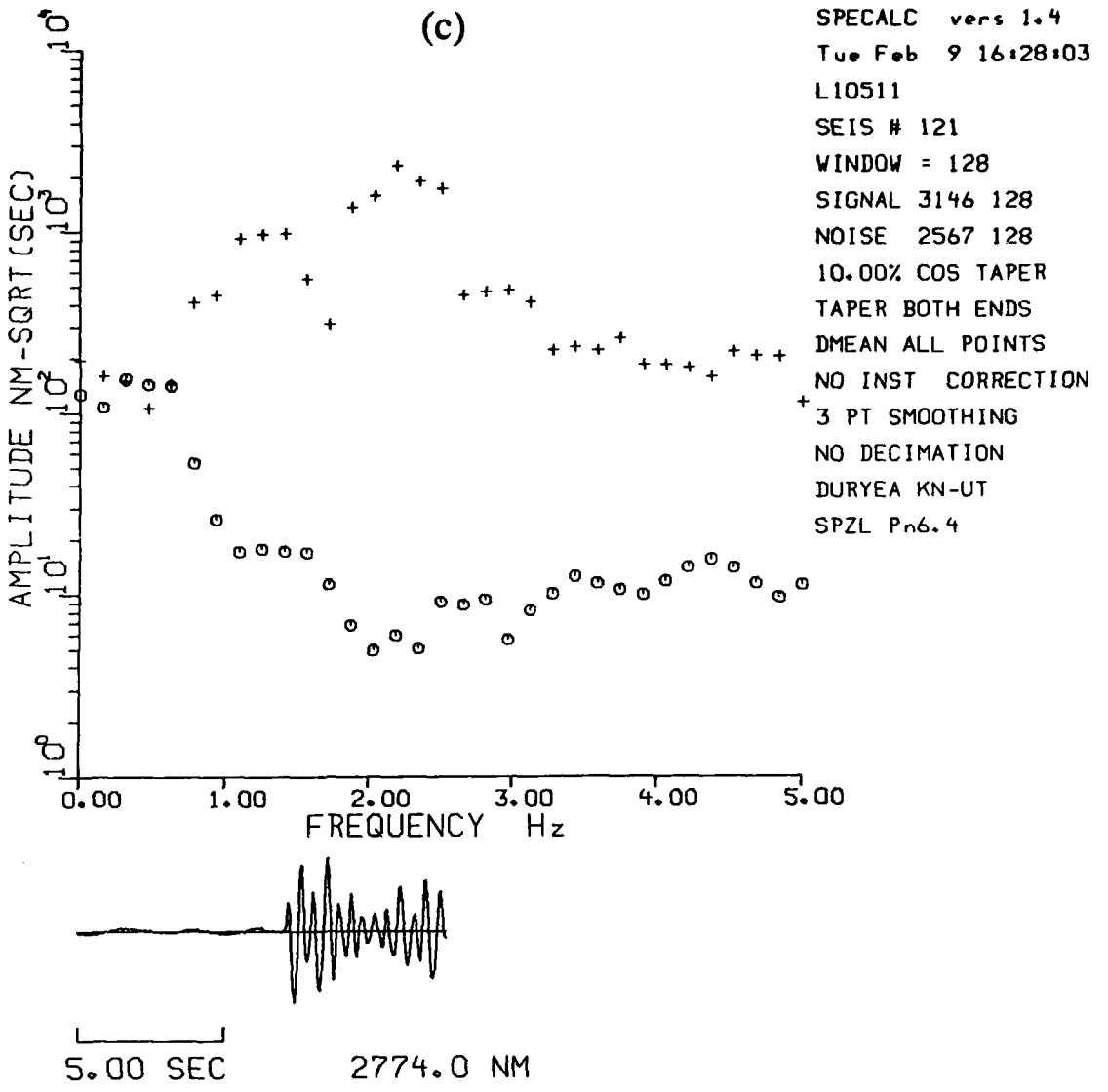

Figure 6. Continued. Vertical-component displacement amplitude spectra (symbol +), not corrected for instrument response, of Pn (based on 6.4 sec long window with 10% cosine taper) recorded at KN-UT for the seven explosions listed in Table III. Spectra of an equal window length of noise are also included (symbol ⊙).

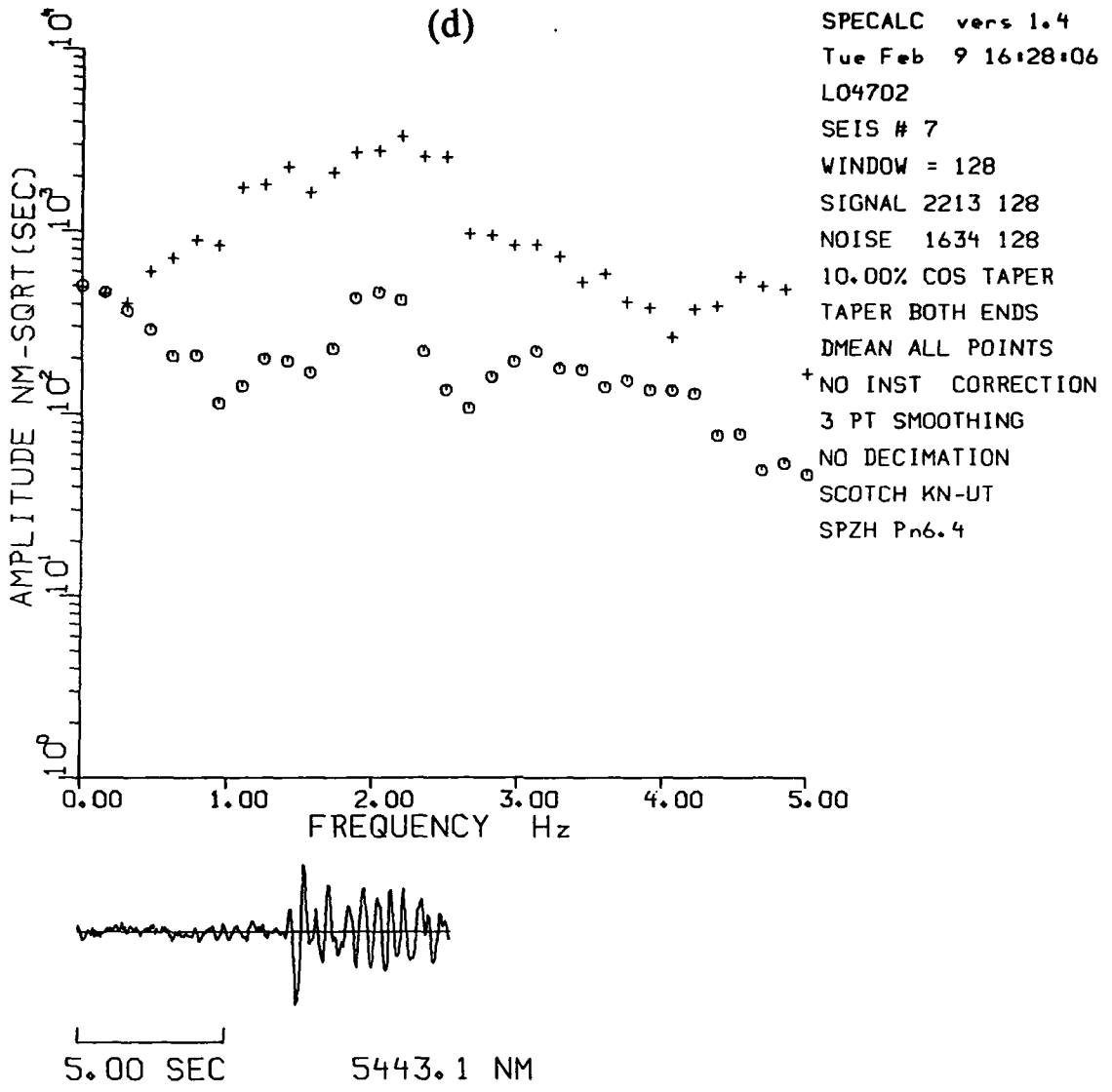

Figure 6. Continued. Vertical-component displacement amplitude spectra (symbol +), not corrected for instrument response, of Pn (based on 6.4 sec long window with 10% cosine taper) recorded at KN-UT for the seven explosions listed in Table III. Spectra of an equal window length of noise are also included (symbol ⊙).

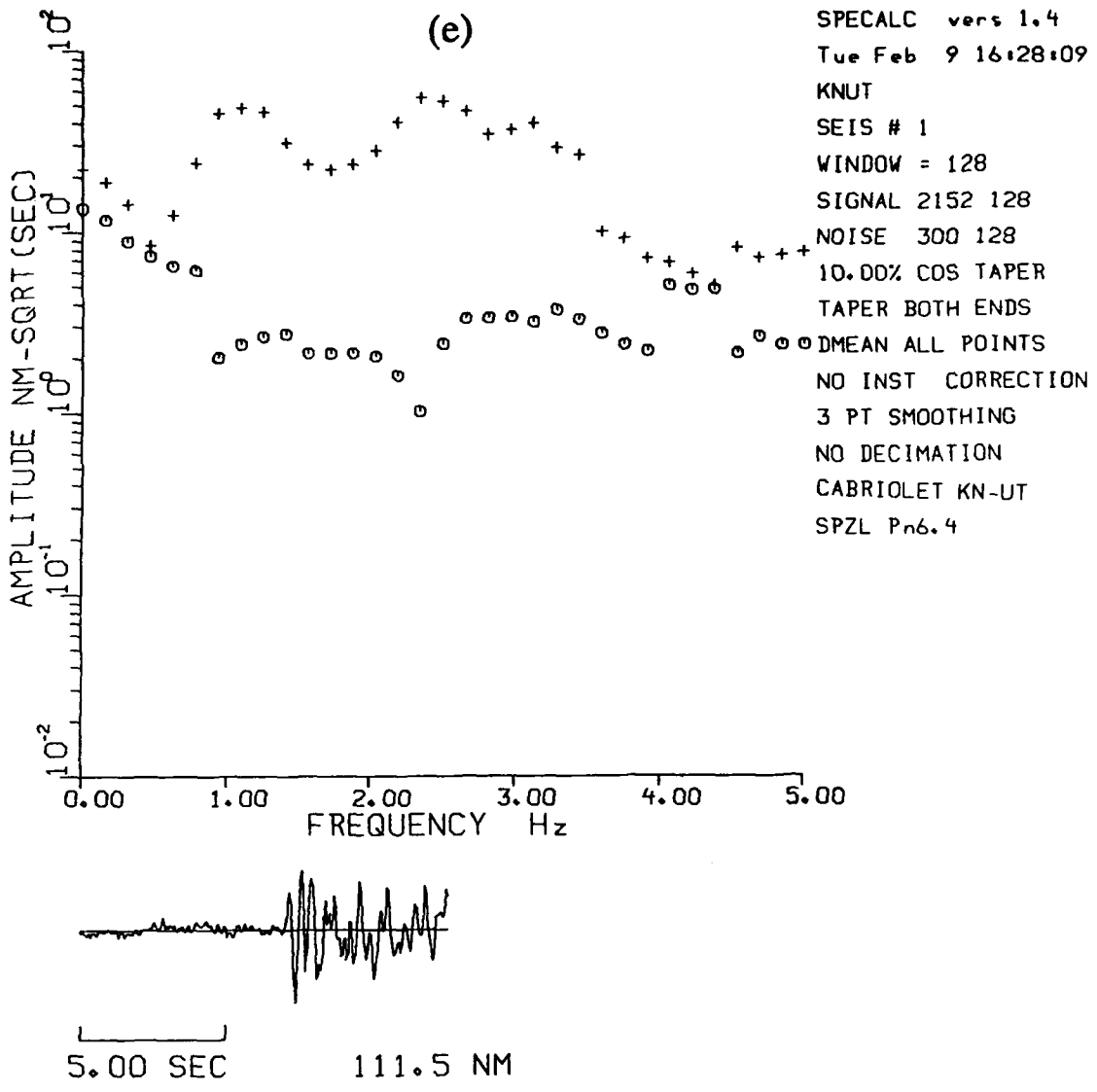

Figure 6. Continued. Vertical-component displacement amplitude spectra (symbol +), not corrected for instrument response, of Pn (based on 6.4 sec long window with 10% cosine taper) recorded at KN-UT for the seven explosions listed in Table III. Spectra of an equal window length of noise are also included (symbol ⊙).

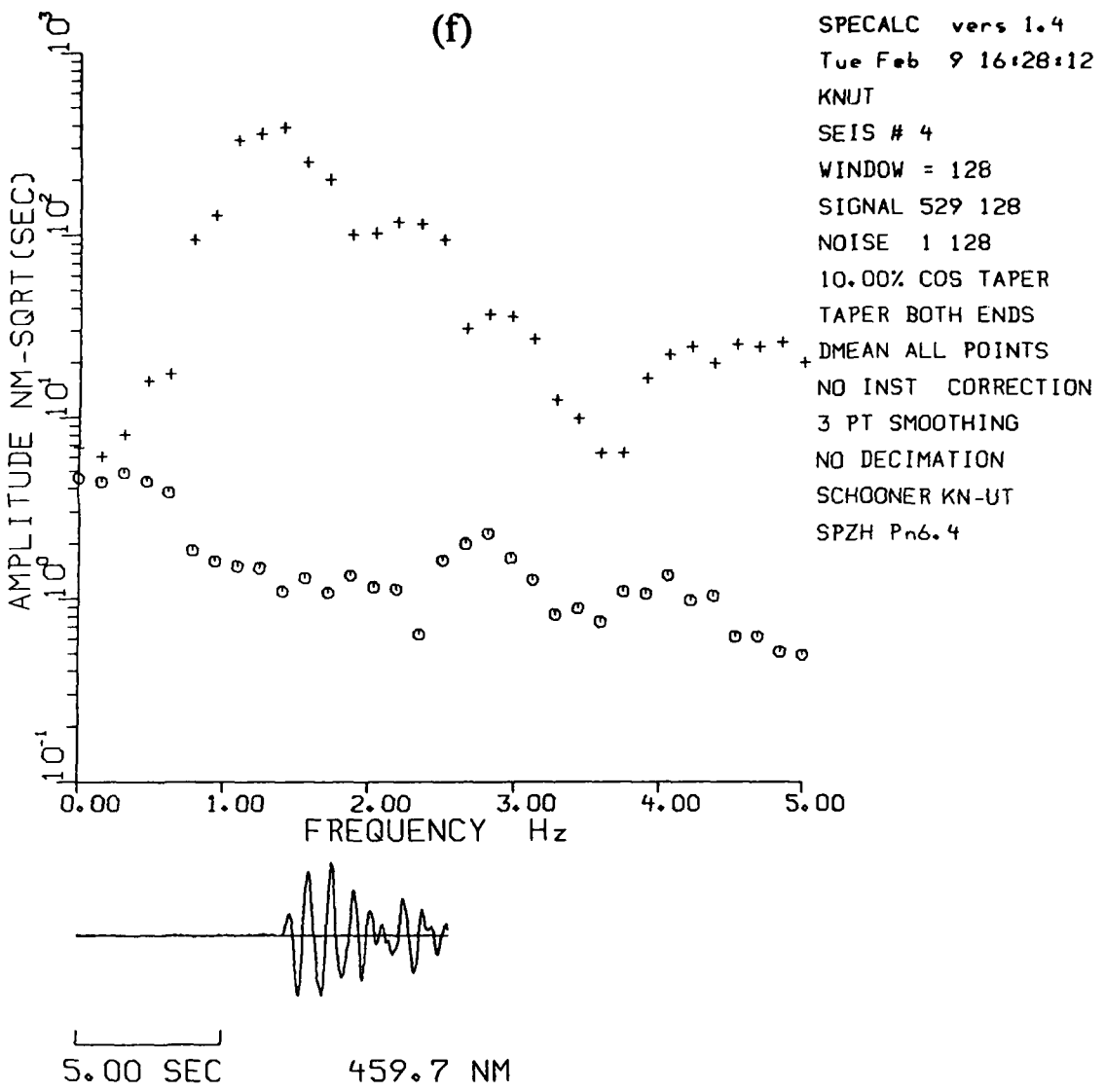

Figure 6. Continued. Vertical-component displacement amplitude spectra (symbol +), not corrected for instrument response, of Pn (based on 6.4 sec long window with 10% cosine taper) recorded at KN-UT for the seven explosions listed in Table III. Spectra of an equal window length of noise are also included (symbol ⊙).

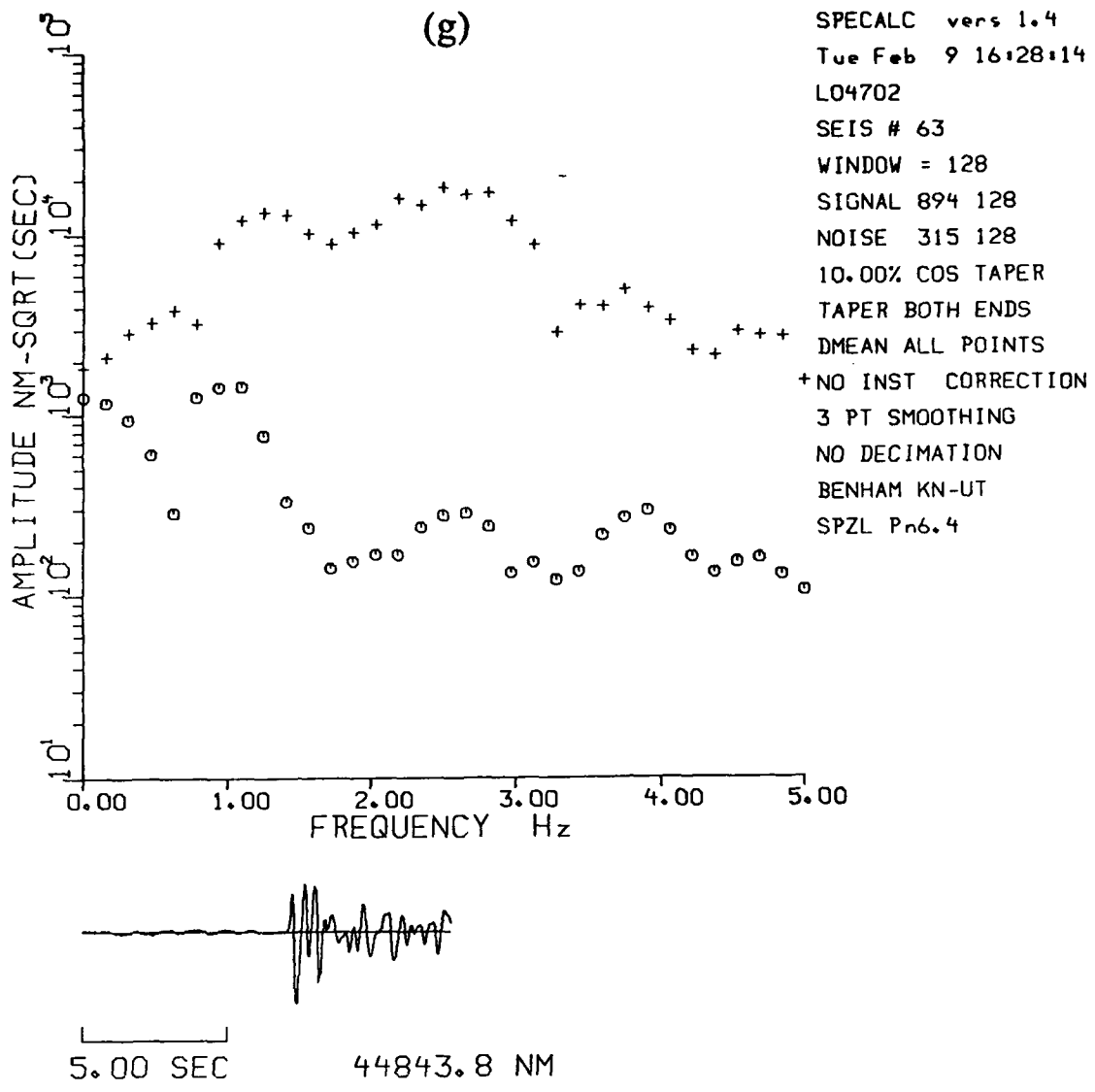

Figure 6. Continued. Vertical-component displacement amplitude spectra (symbol +), not corrected for instrument response, of Pn (based on 6.4 sec long window with 10% cosine taper) recorded at KN-UT for the seven explosions listed in Table III. Spectra of an equal window length of noise are also included (symbol ⊙).

Spectral ratios of Pn with respect to Buteo on the vertical-component records at KN-UT are shown in Figure 7. These are corrected for noise and somewhat smoothed. Most spectra in Figure 6 and the spectral ratios in Figure 7 appear to show the rather systematic modulation with frequency expected because of cancellation by pP. A closer examination indicates, however, many puzzling features that are hard to understand.

Let us first examine the Pn spectra of Buteo and Duryea, both of which were detonated in the same hole but at somewhat different depths. Note that Buteo was vastly overburied. The rather small difference in shot depths of Buteo and Duryea means that, for frequencies less than at least 3 Hz, the propagation paths to KN-UT may be considered to be essentially identical. The spectra of Pn for Buteo (Figure 6a) shows a null at about 1.7 Hz, which agrees well with the value expected on the basis of the shot depth and medium velocity information available for many Pahute Mesa explosions. This means that frequencies lower than at least 2 Hz or so are not substantially influenced by the effects of scattering (both near-source and near-receiver). The explosion Duryea took place in the same hole as Buteo but at shallower depth (see Table 3), and an estimate of its spectral null would suggest a value of about 2.0 to 2.1 Hz, substantially larger than the observed spectral null frequency of 1.7 Hz in Figure 6c. The spectral ratio Duryea/Buteo in Figure 7b also appears to lack the frequency modulation expected for two explosions at different depths but with nearly identical source-receiver propagation paths. One may suggest that the explosion-affected (fractured) volume around the shot-point of Duryea was large enough to slow down the reflected pulse pP during its propagation downward from the free surface. This explanation is, however, not very likely because of the propagation paths involved in Pn and the expected small reduction in the sonic velocity (see Springer, 1974). Non-linear processes, expected to be more prominent for explosions with lower scaled depths, can also retard the downward passage of pP by considerable amounts (Trulio, 1981) and may therefore constitute a more likely explanation. Note also that the near-field pulse from underground explosions may exhibit non-linear behavior at least out to a scaled radius of about 100 $m/kt^{1/3}$ (McCartor and

(a)

REX / BUTEO

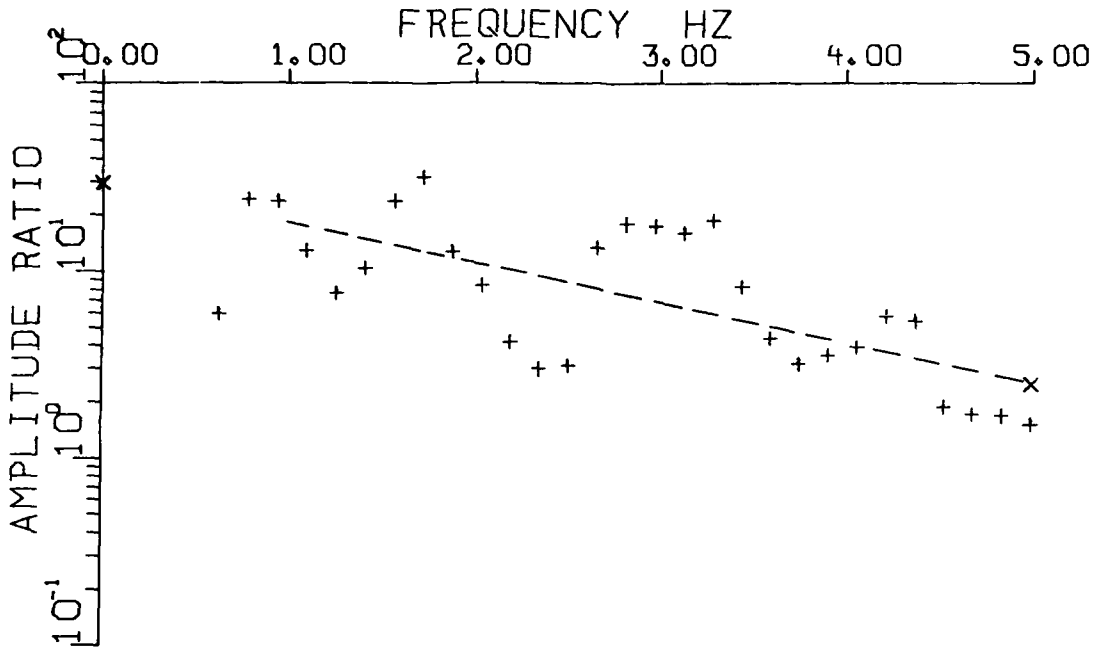

FREQ BAND	SLOPE	+/-	Y INTERC
1.0-5.0	-0.215E+00	4.722E-02	2.966E+01
1.0-4.0	-0.127E+00	7.996E-02	1.889E+01

Figure 7. Spectral ratios of Pn recorded at KN-UT with respect to Buteo for the explosions listed in Table III. The ratios are corrected for noise and points for which *S/N* power ratio is less than 2 are not plotted. The dashed line shows the mean least squares slope over the frequency range of 1.0 to 5.0 Hz. Mean slope, with associated standard deviation (+/-), and the intercept (INTERC) values are indicated for the two frequency ranges of 1.0 to 5.0 Hz and 1.0 to 4.0 Hz.

(b)

DURYEA / BUTEO

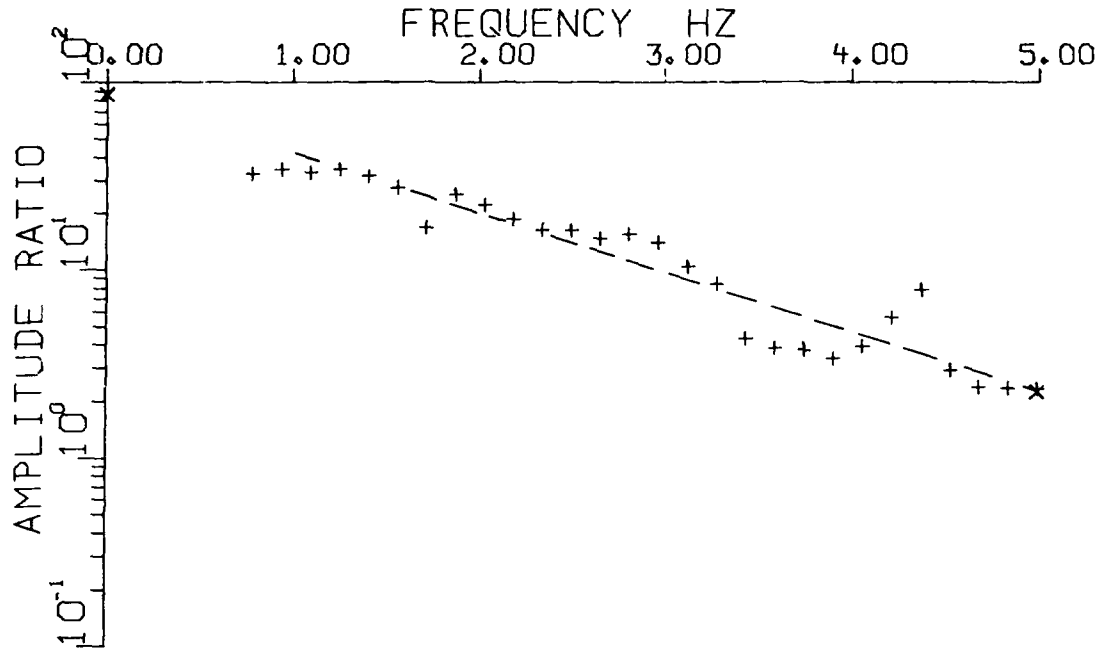

FREQ BAND	SLOPE	+/-	Y INTERC
1.0-5.0	-0.317E+00	2.065E-02	8.639E+01
1.0-4.0	-0.356E+00	2.884E-02	1.043E+02

Figure 7. Continued. Spectral ratios of Pn recorded at KN-UT with respect to Buteo for the explosions listed in Table III. The ratios are corrected for noise and points for which S/N power ratio is less than 2 are not plotted. The dashed line shows the mean least squares slope over the frequency range of 1.0 to 5.0 Hz. Mean slope, with associated standard deviation (+/-), and the intercept (INTERC) values are indicated for the two frequency ranges of 1.0 to 5.0 Hz and 1.0 to 4.0 Hz.

(c)

SCOTCH / BUTEO

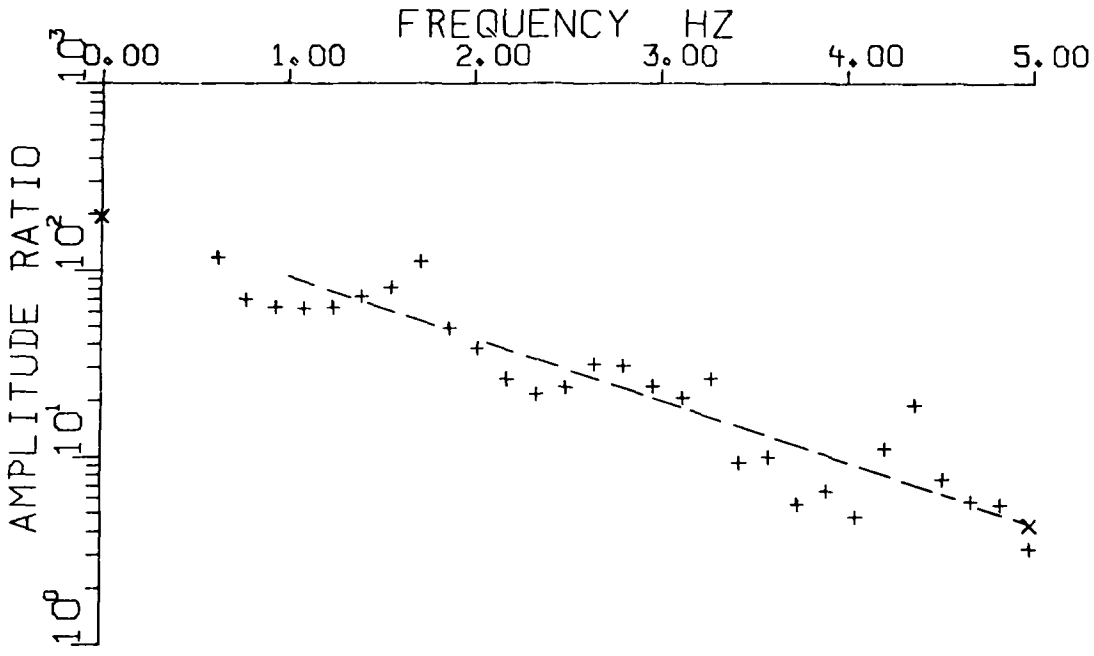

FREQ BAND	SLOPE	+/-	Y INTERC
1.0-5.0	-0.329E+00	2.880E-02	1.947E+02
1.0-4.0	-0.380E+00	3.980E-02	2.490E+02

Figure 7. Continued. Spectral ratios of Pn recorded at KN-UT with respect to Buteo for the explosions listed in Table III. The ratios are corrected for noise and points for which S/N power ratio is less than 2 are not plotted. The dashed line shows the mean least squares slope over the frequency range of 1.0 to 5.0 Hz. Mean slope, with associated standard deviation (+/-), and the intercept (INTERC) values are indicated for the two frequency ranges of 1.0 to 5.0 Hz and 1.0 to 4.0 Hz.

(d)

CABRIOLET / BUTEO

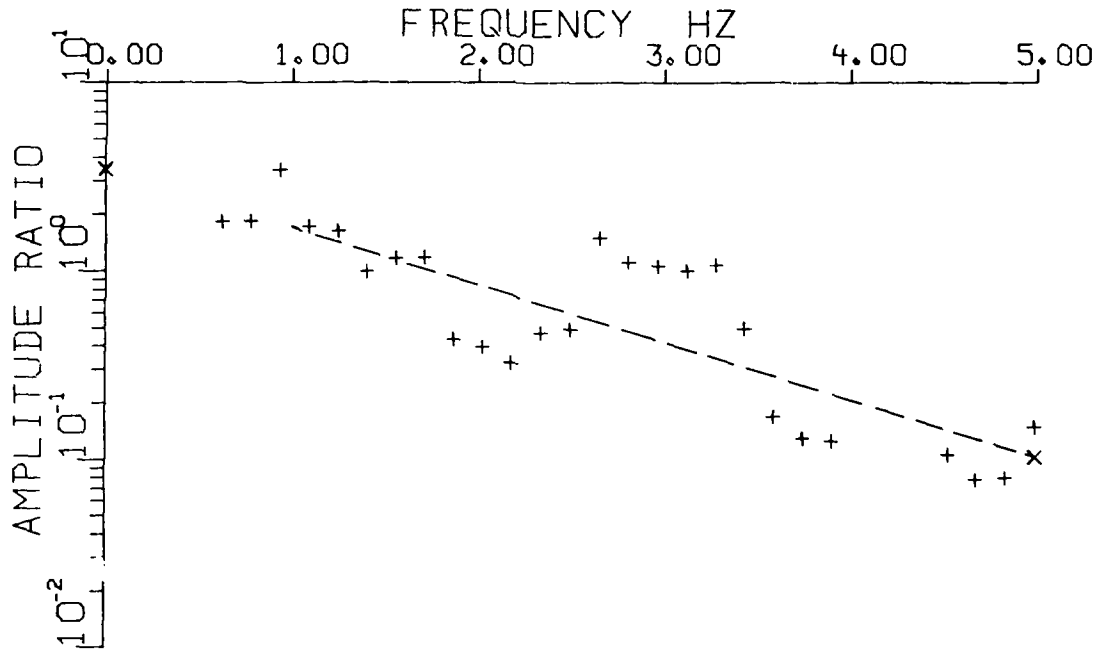

FREQ BAND	SLOPE	+/-	Y INTERC
1.0-5.0	-0.304E+00	4.800E-02	3.462E+00
1.0-4.0	-0.253E+00	7.498E-02	2.688E+00

Figure 7. Continued. Spectral ratios of Pn recorded at KN-UT with respect to Buteo for the explosions listed in Table III. The ratios are corrected for noise and points for which S/N power ratio is less than 2 are not plotted. The dashed line shows the mean least squares slope over the frequency range of 1.0 to 5.0 Hz. Mean slope, with associated standard deviation (+/-), and the intercept (INTERC) values are indicated for the two frequency ranges of 1.0 to 5.0 Hz and 1.0 to 4.0 Hz.

(e)

SCHOONER / BUTEO

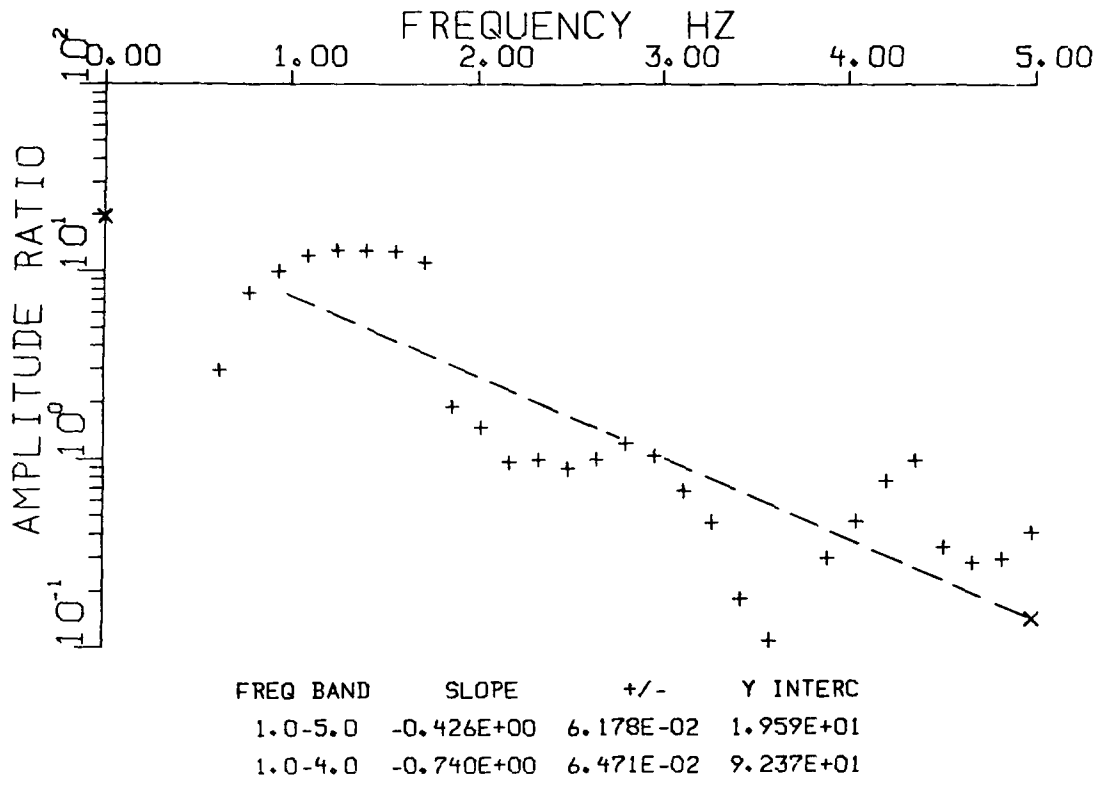

FREQ BAND	SLOPE	+/-	Y INTERC
1.0-5.0	-0.426E+00	6.178E-02	1.959E+01
1.0-4.0	-0.740E+00	6.471E-02	9.237E+01

Figure 7. Continued. Spectral ratios of Pn recorded at KN-UT with respect to Buteo for the explosions listed in Table III. The ratios are corrected for noise and points for which S/N power ratio is less than 2 are not plotted. The dashed line shows the mean least squares slope over the frequency range of 1.0 to 5.0 Hz. Mean slope, with associated standard deviation (+/-), and the intercept (INTERC) values are indicated for the two frequency ranges of 1.0 to 5.0 Hz and 1.0 to 4.0 Hz.

(f)

BENHAM / BUTEO

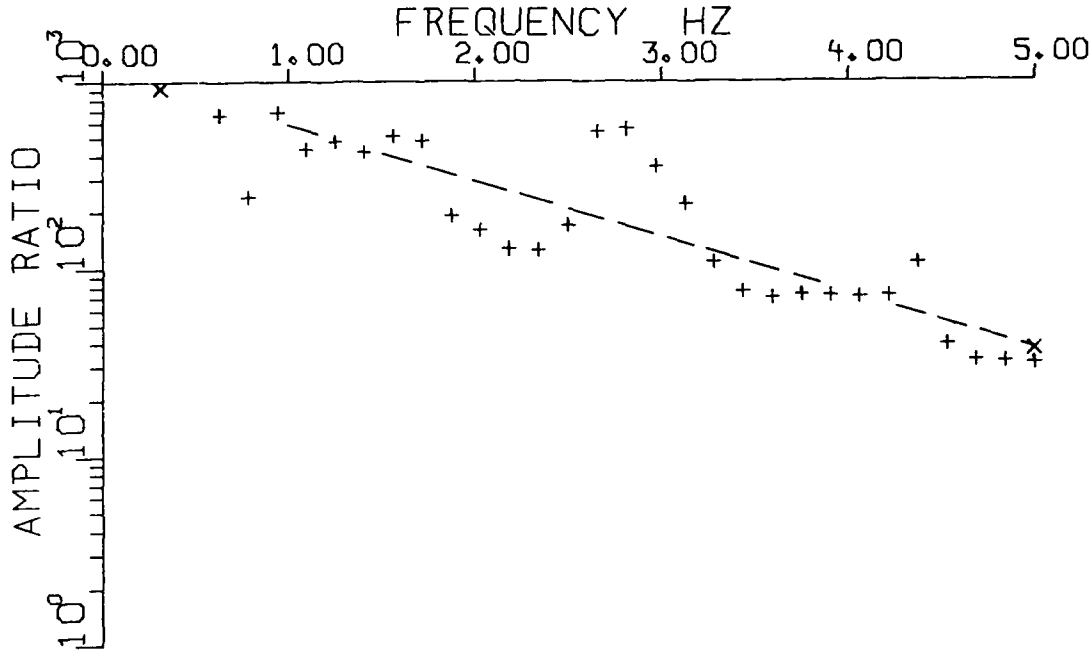

FREQ BAND	SLOPE	+/-	Y INTERC
1.0-5.0	-0.299E+00	3.564E-02	1.156E+03
1.0-4.0	-0.270E+00	6.262E-02	9.959E+02

Figure 7. Continued. Spectral ratios of Pn recorded at KN-UT with respect to Buteo for the explosions listed in Table III. The ratios are corrected for noise and points for which *S/N* power ratio is less than 2 are not plotted. The dashed line shows the mean least squares slope over the frequency range of 1.0 to 5.0 Hz. Mean slope, with associated standard deviation (+/-), and the intercept (INTERC) values are indicated for the two frequency ranges of 1.0 to 5.0 Hz and 1.0 to 4.0 Hz.

Wortman, 1985), a value fairly close to the scaled depth of Duryea (see Table 3). Note also that, for frequencies greater than about 2.5 Hz, the Pn spectra of Buteo shows much stronger frequency modulation than that of Duryea. The finite-difference calculations of McLaughlin *et al.* (1985; see also Figure 5, Der *et al.*, 1985) demonstrate that near-source scattering can "fill" the higher frequency spectral nulls due to cancellation by pP. Greater scattering for Duryea than for Buteo could again be due to significantly larger explosion-fractured volume around the shot point of Duryea. Differences between the Pn spectra of Buteo and Duryea may therefore be due to either non-linear behavior or near-source scattering or to a combination of the two.

The explosion Rex was detonated at a distance of only about 3 km from Buteo, and the two shots have nearly the same depths (see Table 3). This makes it hard to explain the observed spectral nulls for Rex at about 1.3 and 2.5 Hz in Figure 6b and the large modulation, even at low frequencies, in the observed spectral ratio Rex/Buteo in Figure 7a. Differences in near-source scattering alone are unlikely to explain the large low-frequency differences between the spectra of Rex and Buteo (see Figure 5 of Der *et al.*, 1985, wherein the low-frequency spectra are not much contaminated by the scattered arrivals). Inelastic processes may again provide a more logical explanation. In addition to Buteo and Duryea, the cratering explosion Cabriolet at depth of only 52 m and Benham with shot depth of 1402 m also indicate spectral nulls at about 1.7 Hz (see Figures 6e and 6g). It is hard to explain these observations without assuming non-linear processes and scattering due to complex near-source structures.

Figure 8 shows the Pn spectra of Mast and Stilton at the three broadband digital stations Elko, Kanab (the same location as KN-UT), and Landers; the signals at the fourth station Mina were clipped. The shot medium for Mast was considerably harder rock (work-point velocity of about 4.2 km/sec) than for Stilton (work-point velocity about 2.6 km/sec). The three stations are approximately north, east, and south of NTS at distances of about 400, 300, and 300 km, respectively. On the basis of their

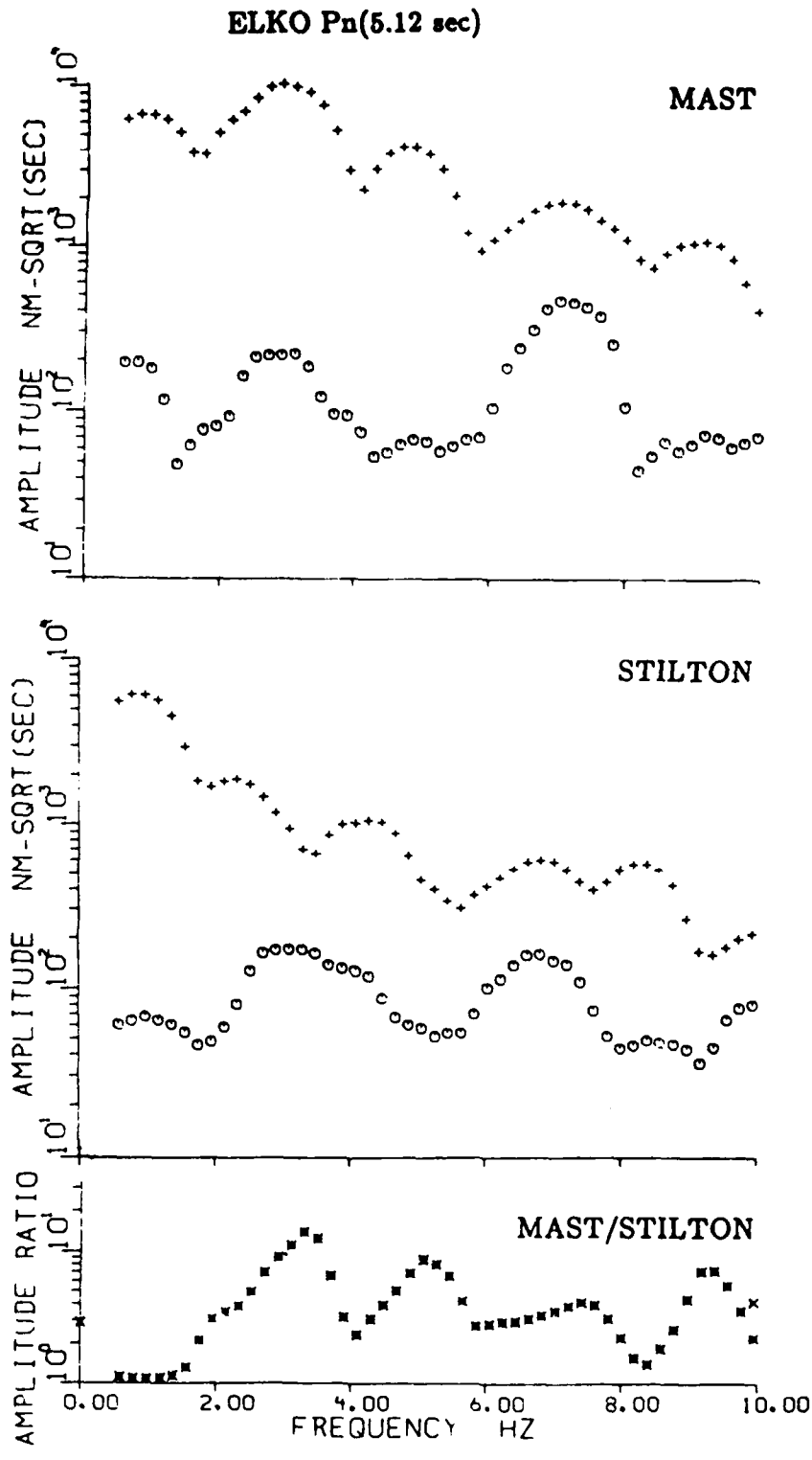

Figure 8a. Spectra of Pn (based on 5.12 sec long window) for the Pahute Mesa explosions Mast and Stilton recorded at the broadband digital station Elko. The spectral ratios Mast/Stilton, corrected for noise, are also shown.

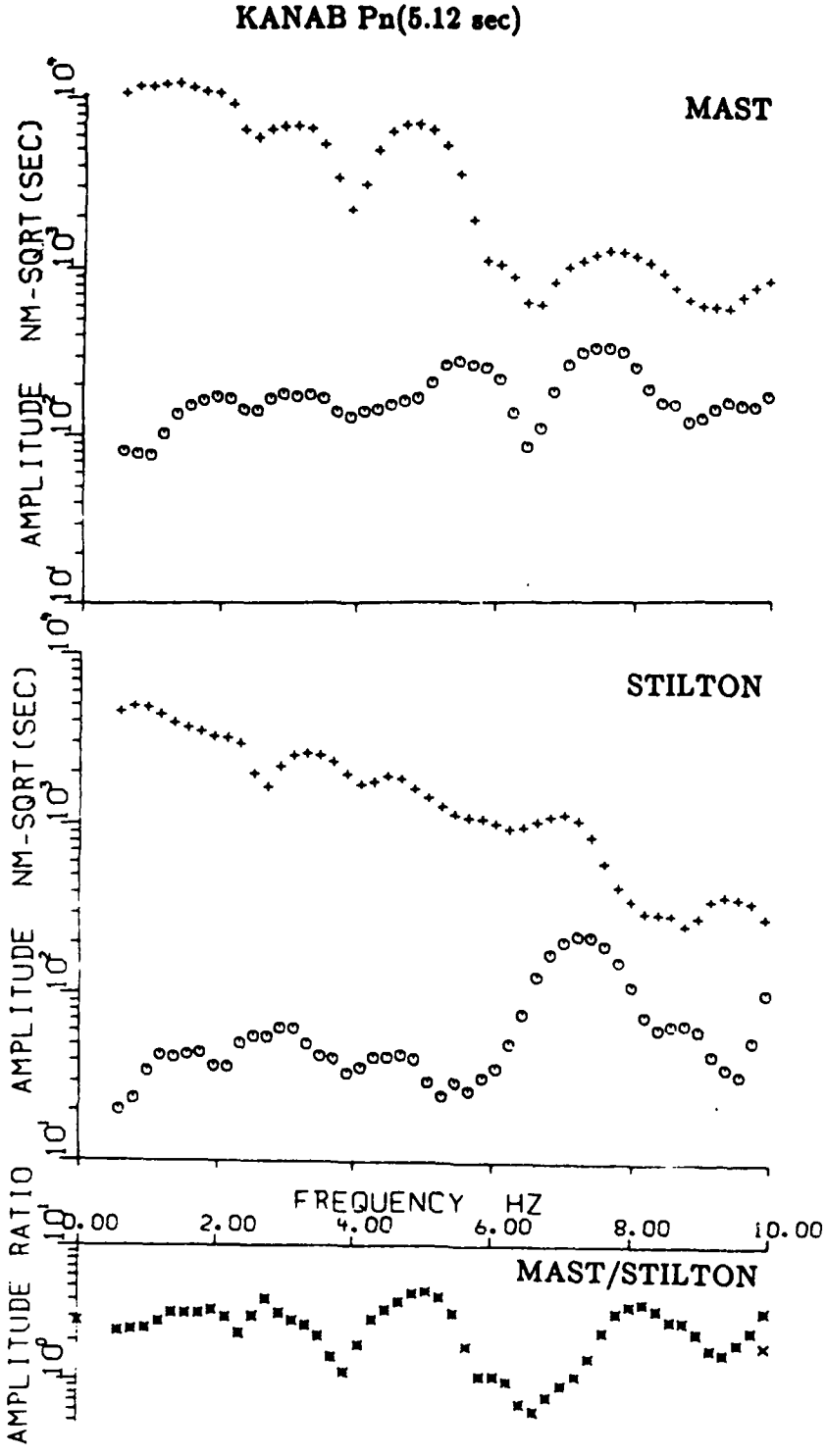

Figure 8b. Spectra of Pn (based on 5.12 sec long window) for the Pahute Mesa explosions Mast and Stilton recorded at the broadband digital station Kanab. The spectral ratios Mast/Stilton, corrected for noise, are also shown.

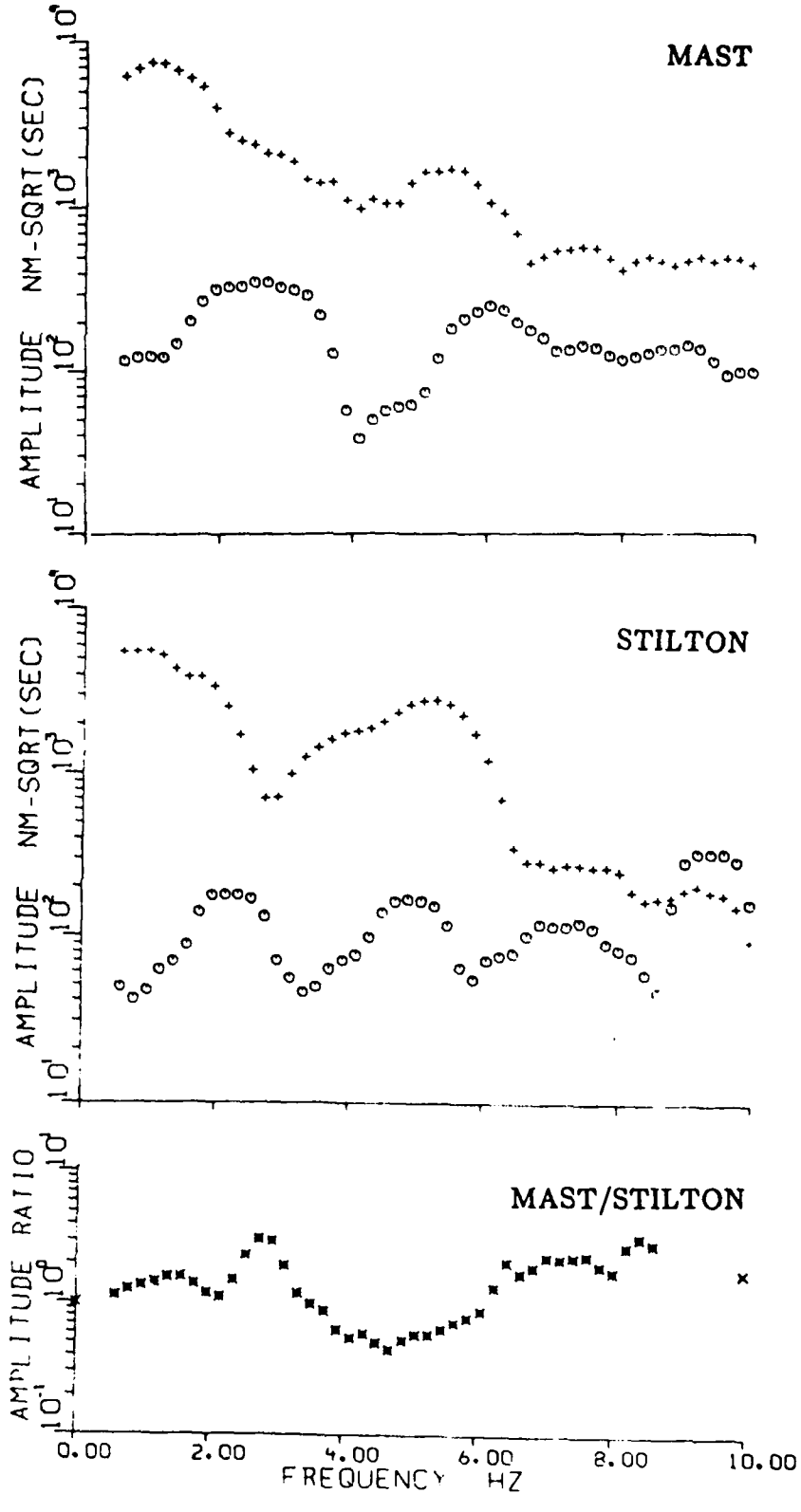

Figure 8c. Spectra of Pn (based on 5.12 sec long window) for the Pahute Mesa explosions Mast and Stilton recorded at the broadband digital station Landers. The spectral ratios Mast/Stilton, corrected for noise, are also shown.

known depths and overburden velocities, the spectral nulls due to pP cancellation should occur at about 2.1, 4.2, 6.3, ... Hz for Mast and 1.5, 3.0, 4.5, ... Hz for Stilton. The observed spectra of Mast at the three stations show modulation in fair agreement with what should be expected. The same, however, cannot be said for the results from Stilton. These differences may again be due to non-linear effects which are medium-dependent and less pronounced for harder rocks (Trulio, 1981). The spectral ratios, Mast/Stilton, also shown in Figure 8, indicate fairly large differences from one station to another. Mast and Stilton are separated by less than 20 km, so their paths to the three stations should not be much different, and the spectral ratios Mast/Stilton should be essentially free from the effects of local (receiver) structure. Differences in the spectral ratios at the three sites therefore imply large azimuthal variations in the source spectra of Pn.

Large lateral variations in elastic parameters seem to exist within the Pahute Mesa region. Figure 9 shows the location of 51 Pahute Mesa explosions along with all available data on overburden velocity (*i.e.*, average shot-point to surface velocity) from 33 explosions. Extreme lateral and vertical variations in velocity, probably due to the presence of alternating layers of various tuffs and rhyolites of irregular thicknesses, are evident. For example, in the source region of Mast, with the highest reported overburden velocity of 3.9 km/sec, several high velocity rhyolite layers with velocity as high as 4.6 km/sec intersect the overburden (Nancy Howard, written communication). Figure 9 indicates an overburden velocity of only 2.0 km/sec at an explosion site only about 500 m from the ground zero for Mast. Although the shot depths for the two explosions are different, the high velocity rhyolites near the Mast location have to be very thin or absent at the neighboring shot location. It seems therefore likely that the large differences in the spectra of Pn, observed even for explosions that are close, are due to a combination of non-linear effects of inelastic processes and complex near-source structure with strong lateral variations.

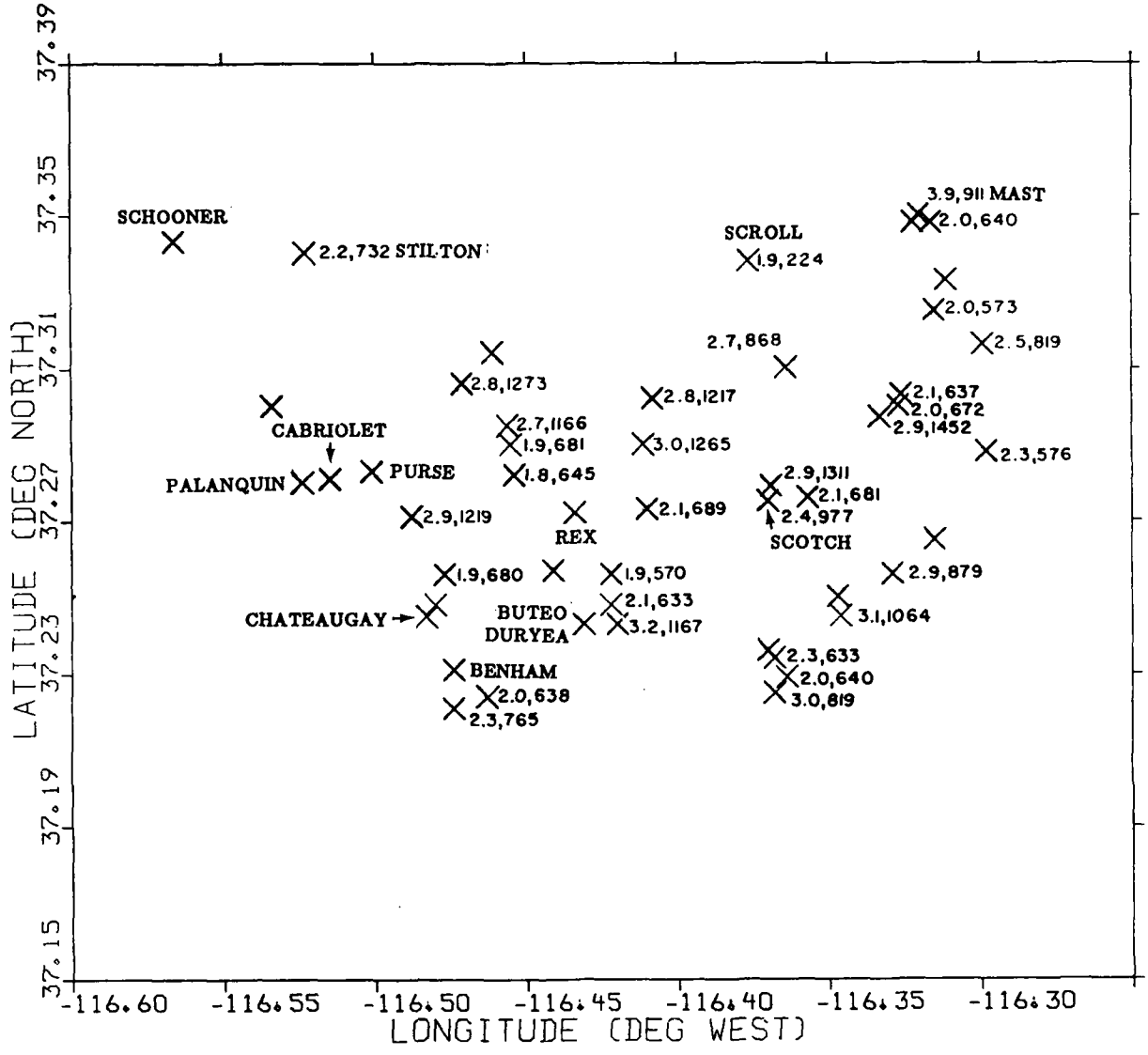

Figure 9. Location map of all (51) announced Pahute Mesa explosions up to 24 June 1982. The available average overburden velocity (km/sec) and shot depth (m) are indicated and all (13) events cited in the text are identified.

A comparison of the Pn spectra (Figure 6) and the spectral ratios (Figure 7) of the two cratering and five non-cratering explosions shows no obvious differences. This seems to imply that the pP arrivals from cratering and non-cratering explosions are not much different. But the cratering explosions are not expected to have well-defined pP arrivals, because there is no true reflection of energy at the free surface. Perhaps the effects of non-linear behavior and complex near-source structure dominate over those distinguishing between cratering and non-cratering explosions.

DISCUSSION AND CONCLUSION

A comparison of the amplitudes of regional phases Pn, Pg, and Lg as well as the ratio Pmax/Pa from cratering and non-cratering explosions failed to show any systematic differences. These amplitudes appear to be dependent more on the characteristics of the shot medium and near-source environment than on whether the explosion is cratering or not. These results are not surprising, in view of the extreme variability of regional phases noted in several earlier studies (*e.g.*, Springer and Denny, 1976; Patton and Vergino, 1981; Gupta *et al.*, 1984). An important contributor to the large variability is generally believed to be near-source scattering (Gupta and Blandford, 1983; Hill and Levander, 1984; Der *et al.*, 1984, McLaughlin *et al.*, 1985).

The spectra of Pn show no obvious distinction between cratering and contained explosions. A comparison of data from closely spaced shots suggests Pn to be strongly influenced by the effects of non-linear behavior and complex near-source structure. Whereas the Pn spectrum of the vastly overburied explosion Buteo showed definite evidence of cancellation by pP, the details of spectral modulation for most other explosions indicate significant differences from what would be expected on the basis of an idealized compressional point source. It seems that, although pP is a significant contributor to Pn for most explosions, as evidenced by nearly periodic undulations in the Pn spectra of several explosions, it can easily be masked beyond recognition by the effects of the non-linear behavior of rocks around the shot point and scattering. Our results regarding the role of pP in the composition of Pn are in general agreement with those of Der *et al.* (1985), obtained by using a multichannel deconvolution method, for teleseismic P and pP from NTS explosions. It is recommended that more regional data, especially from closely spaced shots, be analyzed to explore further the roles of non-linear behavior and near-source scattering in the make-up of regional phases.

REFERENCES

Blandford, R., R. Hartenberger, and R. Naylor (1981). Regional amplitude-distance relations, discrimination and detection, *VSC-TR-81-15*, Teledyne Geotech, Alexandria, Virginia.

Blandford, R. R. and P. Klouda (1980). Magnitude-yield results at the Tonto Forest Observatory, *in* Studies of seismic wave characteristics at regional distances, *AL-80-1*, Teledyne Geotech, Alexandria, Virginia.

Der, Z. A., M. E. Marshall, A. O'Donnell, and T. W. McElfresh (1984). Spatial coherence structure and attenuation of the Lg phase, site effects, and interpretation of the Lg coda, *Bull. Seism. Soc. Am., 74*, 1125-1147.

Der, Z. A., A. O'Donnell, T. W. McElfresh, R. Jutila, J. A. Burnetti, M. Marshall, M. Silk, and E. Gordon (1982). A study of seismic wave propagation at regional distances in five areas of the world, *VSC-TR-82-14*, Teledyne Geotech, Alexandria, Virginia.

Der, Z. A., R. H. Shumway, A. C. Lees, and E. Smart (1985). Multichannel deconvolution of P waves at seismic arrays, *TGAL-85-4*, Teledyne Geotech, Alexandria, Virginia.

Gupta, I. N. and R. R. Blandford (1983). A mechanism for generation of short-period transverse motion from explosions, *Bull. Seism. Soc. Am., 73*, 571-591.

Gupta, I. N., J. A. Burnetti, R. A. Wagner, and M. Marshall (1984). Discrimination between quarry blasts, nuclear explosions and earthquakes, *TGAL-TR-84-1*, Teledyne Geotech, Alexandria, Virginia.

Hill, N. R. and A. R. Levander (1984). Resonances of low-velocity layers with lateral variations, *Bull. Seism. Soc. Am. 74*, 521-537.

McCartor, G. D. and W. R. Wortman (1985). Experimental and analytic characterization of nonlinear seismic attenuation, *MRC-R-900*, Mission Research Corporation, Santa Barbara, California.

McLaughlin, K. L., L. M. Anderson, Z. A. Der, and T. W. McElfresh (1985). Investigation of the effects of local geologic structure on NTS waveforms for Yucca Valley, 2-dimensional finite difference calculations, *Semi-annual Report: AFOSR (Jan. 1, 1985)*, Teledyne Geotech, Alexandria, Virginia.

Nuttli, O. W. (1983). A methodology for obtaining seismic yield estimates of underground explosions using short-period Lg waves, *in* Attenuation of Seismic Waves at Regional Distances, Semi-annual Report (31 March 1983), Saint Louis University, St. Louis, Missouri.

Patton, H. J. and E. S. Vergino (1981). Source effects on surface waves from Nevada Test Site explosions, *UCRL-53247*, Lawrence Livermore National Laboratory, Livermore, California.

Ringdal, F. (1976). Maximum-likelihood estimation of seismic magnitude, *Bull. Seism. Soc. Am., 66*, 789-802.

Springer, D. L. (1974). Secondary sources of seismic waves from underground nuclear explosions, *Bull. Seism. Soc. Am., 64*, 581-594.

Springer, D. L. and M. D. Denny (1976). Seismic spectra of events at regional distances, *UCRL-52048*, Lawrence Livermore Laboratory, Livermore, California.

Springer, D. L. and R. L. Kinnaman (1971). Seismic source summary for U. S. underground nuclear explosions, 1961-1970, *Bull. Seism. Soc. Am., 61*, 1073-1098.

Trulio, J. G. (1981). State of the art assessment: seismic yield determination, A technical assessment of seismic yield estimation, Appendix (Part 1 of 2), *DARPA-NMR-81-01*, Defense Advanced Research Projects Agency, Arlington, Virginia.

(THIS PAGE INTENTIONALLY LEFT BLANK)

DISTRIBUTION LIST
FOR UNCLASSIFIED REPORTS
DARPA-FUNDED PROJECTS
(Last Revised: 3 Mar 1988)

RECIPIENT	NO. OF COPIES
DEPARTMENT OF DEFENSE	
DARPA/GSD ATTN: Dr. R. Alewine and Dr. R. Blandford 1400 Wilson Boulevard Arlington, VA 22209-2308	2
DARPA/PM 1400 Wilson Boulevard Arlington, VA 22209-2308	1
Defense Intelligence Agency Directorate for Scientific and Technical Intelligence Washington, D.C. 20301	1
Defense Nuclear Agency Shock Physics Washington, D.C. 20305-1000	1
Defense Technical Information Center Cameron Station Alexandria, VA 22314	2
DEPARTMENT OF THE AIR FORCE	
AFGL/LWH ATTN: Dr. J. Cipar and Mr. J. Lewkowicz Terrestrial Sciences Division Hanscom AFB, MA 01731-5000	2
AFOSR/NPG ATTN: Director Bldg. 410, Room C222 Bolling AFB, Washington, D.C. 20332	1

AFTAC/DA 1
ATTN: STINFO Officer
Patrick AFB, FL 32925-6001

AFTAC/TT 3
Patrick AFB, FL 32925-6001

AFWL/NTESG 1
Kirtland AFB, NM 87171-6008

DEPARTMENT OF THE NAVY

NORDA 1
ATTN: Dr. J.A. Ballard
Code 543
NSTL Station, MS 39529

DEPARTMENT OF ENERGY

Department of Energy 1
ATTN: Mr. Max A. Koontz (DP-52)
International Security Affairs
1000 Independence Avenue
Washington, D.C. 20545

Lawrence Livermore National Laboratory 2
ATTN: Dr. J. Hannon and Dr. M. Nordyke
University of California
P.O. Box 808
Livermore, CA 94550

Los Alamos Scientific Laboratory 2
ATTN: Dr. K. Olsen and Dr. T. Weaver
P.O. Box 1663
Los Alamos, NM 87544

Sandia Laboratories 1
ATTN: Mr. P. Stokes
Geosciences Department 1255
Albuquerque, NM 87185

OTHER GOVERNMENT AGENCIES

Central Intelligence Agency 1
ATTN: Dr. L. Turnbull
OSI/NED, Room 5G48
Washington, D.C. 20505

U.S. Arms Control and Disarmament Agency 1
ATTN: Dr. M. Eimer
Verification and Intelligence Bureau, Rm 4953
Washington, D.C. 20451

U.S. Arms Control and Disarmament Agency 1
ATTN: Mrs. M. Hoinkes
Multilateral Affairs Bureau, Rm 5499
Washington, D.C. 20451

U.S. Geological Survey 1
ATTN: Dr. T. Hanks
National Earthquake Research Center
345 Middlefield Road
Menlo Park, CA 94025

U.S. Geological Survey 1
ATTN: Dr. R. Masse
Global Seismology Branch
Box 25046, Stop 967
Denver Federal Center
Denver, CO 80225

UNIVERSITIES

Boston College 1
ATTN: Dr. A. Kafka
Western Observatory
381 Concord Road
Weston, MA 02193

California Institute of Technology 1
ATTN: Dr. D. Harkrider
Seismological Laboratory
Pasadena, CA 91125

Columbia University 1
ATTN: Dr. L. Sykes
Lamont-Doherty Geological Observatory
Palisades, NY 10964

Cornell University 1
ATTN: Dr. M. Barazangi
INSTOC
Snee Hall
Ithaca, NY 14853

Harvard University 1
ATTN: Dr. J. Woodhouse
Hoffman Laboratory
20 Oxford Street
Cambridge, MA 02138

Massachusetts Institute of Technology 3
ATTN: Dr. S. Soloman, Dr. N. Toksoz, and Dr. T. Jordan
Department of Earth and Planetary Sciences
Cambridge, MA 02139

Southern Methodist University 1
ATTN: Dr. E. Herrin
Geophysical Laboratory
Dallas, TX 75275

State University of New York at Binghamton 1
ATTN: Dr. F. Wu
Department of Geological Sciences
Vestal, NY 13901

St. Louis University 2
ATTN: Dr. O. Nuttli and Dr. R. Herrmann
Department of Earth and Atmospheric Sciences
3507 Laclede
St. Louis, MO 63156

The Pennsylvania State University 1
ATTN: Dr. S. Alexander
Geosciences Department
403 Deike Building
University Park, PA 16802

University of Arizona 1
ATTN: Dr. T. Wallace
Department of Geosciences
Tucson, AZ 85721

University of California, Berkeley 1
ATTN: Dr. T. McEvilly
Department of Geology and Geophysics
Berkeley, CA 94720

University of California Los Angeles 1
ATTN: Dr. L. Knopoff
405 Hilgard Avenue
Los Angeles, CA 90024

University of California, San Diego 1
ATTN: Dr. J. Orcutt
Scripps Institute of Oceanography
La Jolla, CA 92093

University of Colorado 1
ATTN: Dr. C. Archambeau
CIRES
Boulder, CO 80309

University of Illinois 1
ATTN: Dr. S. Grand
Department of Geology
1301 West Green Street
Urbana, IL 61801

University of Michigan 1
ATTN: Dr. T. Lay
Department of Geological Sciences
Ann Arbor, MI 48109-1063

University of Nevada 1
ATTN: Dr. K. Priestley
Mackay School of Mines
Reno, NV 89557

University of Southern California 1
ATTN: Dr. K. Aki
Center for Earth Sciences
University Park
Los Angeles, CA 90089-0741

DEPARTMENT OF DEFENSE CONTRACTORS

Applied Theory, Inc. 1
ATTN: Dr. J. Trulio
930 South La Brea Avenue
Suite 2
Los Angeles, CA 90036

Center for Seismic Studies 2
ATTN: Dr. C. Romney and Mr. R. Perez
1300 N. 17th Street, Suite 1450
Arlington, VA 22209

ENSCO, Inc.
ATTN: Mr. G. Young 1
5400 Port Royal Road
Springfield, VA 22151

ENSCO, Inc. 1
ATTN: Dr. R. Kemerait
445 Pineda Court
Melbourne, FL 32940

Gould Inc. 1
ATTN: Mr. R. J. Woodard
Chesapeake Instrument Division
6711 Baymeado Drive
Glen Burnie, MD 21061

Pacific Sierra Research Corp. 1
ATTN: Mr. F. Thomas
12340 Santa Monica Boulevard
Los Angeles, CA 90025

Rockwell International 1
ATTN: B. Tittmann
1049 Camino Dos Rios
Thousand Oaks, CA 91360

Rondout Associates, Inc. 1
ATTN: Dr. P. Pomeroy
P.O. Box 224
Stone Ridge, NY 12484

Science Applications, Inc. 1
ATTN: Dr. T. Bache, Jr.
P.O. Box 2351
La Jolla, CA 92038

Science Horizons 2
ATTN: Dr. T. Cherry and Dr. J. Minster
710 Encinitas Blvd.
Suite 101
Encinitas, CA 92024

Sierra Geophysics, Inc. 2
ATTN: Dr. R. Hart and Dr. G. Mellman
11255 Kirkland Way
Kirkland, WA 98124

SRI International 1
ATTN: Dr. A. Florence
333 Ravensworth Avenue
Menlo Park, CA 94025

S-Cubed, A Division of 1
Maxwell Laboratories Inc.
ATTN: Dr. S. Day
P.O. Box 1620
La Jolla, CA 92038-1620

S-Cubed, A Division of
Maxwell Laboratories Inc.
ATTN: Mr. J. Murphy
11800 Sunrise Valley Drive
Suite 1212
Reston, VA 22091 — 1

Teledyne Geotech
ATTN: Dr. Z. Der and Mr. W. Rivers
314 Montgomery Street
Alexandria, VA 22314 — 2

Woodward-Clyde Consultants
ATTN: Dr. L. Burdick and Dr. J. Barker
556 El Dorado St.
Pasadena, CA 91105 — 2

NON-U.S. RECIPIENTS

National Defense Research Institute FOA 290
ATTN: Dr. O. Dahlman
Box 27322
S-10254 Stockholm, Sweden — 1

Blacknest Seismological Center
ATTN: Mr. P. Marshall
Atomic Weapons Research Establishment
UK Ministry of Defence
Brimpton, Reading, Berks. RG7-4RS
United Kingdom — 1

NTNF NORSAR
ATTN: Dr. F. Ringdal
P.O. Box 51
N-2007 Kjeller
Norway — 1

OTHER DISTRIBUTION

To be determined by the project office — 9